

UTRECHT UNIVERSITY



MASTER THESIS

October, 2021

**Quantitative Characterization and
Conceptual Modeling of a Heterogeneous
Dinantian Carbonate Reservoir:
Implications on the Associated
Geothermal Energy Potential Assessment
of the Luttelgeest Isolated Platform**

Author:

Freek Leendert MODDERMAN

Supervisors:

Prof. dr. Fadi Henri NADER

Prof. dr. Rudy SWENNEN

Abstract

The Carboniferous Dinantian carbonates of the Dutch onshore may be a target for geothermal application. With a positive temperature anomaly of 150-200 °C at 4-5 km depth, geothermal energy generation from the Luttelgeest platform is an enterprise that could be considered. It comprises an isolated carbonate platform system, which is located in the Dutch onshore subsurface below the province of Flevoland and is encountered at 4355 to 5123 m depth. Only one well, Luttelgeest-01 (LTG-01) penetrates the succession. Previous work on the area has shown that the carbonates comprise a fine-grained, muddy matrix with an intergranular porosity close to 0% which initially would make fluid convection impossible. The margins, however, are heavily fractured and might provide pathways for fluid flow. In this study, the geothermal potential of the platform has been evaluated by the analysis of core, log, well data of LTG-01, together with 2D seismic data and analogues. Firstly, the goal is to design a workflow and apply it to reach a set objective on these Dinantian carbonates, with the idea that the same workflow could be applied to similar cases elsewhere. Secondly, a conceptual model for fluid flow in the platform through a fault plane is proposed, as well as stratigraphic boundaries between sequence cycles in the platform. This model reveals the considerable possibilities of the Luttelgeest platform for ultra deep geothermal development.

Contents

1	Introduction	3
1.1	Geothermal energy and the energy transition	3
1.2	Potential of Dinantian carbonates in the Netherlands	3
1.3	Study objective	5
2	Geological Setting	6
2.1	Tectonic setting	6
2.1.1	Caledonian and Variscan orogeny	6
2.1.2	Devonian	6
2.1.3	Early Carboniferous (Dinantian)	8
2.1.4	Late Carboniferous (Silesian)	10
2.1.5	Permian	10
2.1.6	Mesozoic	11
2.1.7	Cenozoic	11
2.2	Stratigraphic distribution of the Dinantian in the Dutch subsurface	11
2.3	The Luttelgeest platform	13
3	Data and Methodologies	13
3.1	Literature study on available datasets	13
3.2	Quantitative petrography	14
3.3	Seismic interpretation, facies associations and well log integration	14
4	Synthesis of Previous Work	15
4.1	Introduction	15
4.2	Sedimentology	15
4.3	Sequence stratigraphy	17
4.4	Diagenesis and fracture analysis	17
4.5	Global Dinantian platform models	20
5	Results and Interpretations	21
5.1	Petrographic analysis	21
5.2	Quantitative petrography	22
5.3	Well log and FMI integration	24
5.4	Seismic interpretations	27
5.4.1	Faults and seismic horizons	27
5.4.2	Seismic facies associations	30
6	Discussion	32
6.1	Dolomitization and impact on reservoir properties	32
6.2	Implications of fractures as potential flow pathways	33
6.3	Implications of stratigraphic boundaries as potential flow pathways	36
6.4	Proposed conceptual model for potential fluid flow pathways through Dinantian carbonate reservoirs	36
6.5	Uncertainties	36
7	Conclusions	38
	Acknowledgements	39
	References	39
	Appendices	43
	Appendix A: Lithostratigraphic nomenclature of the Dutch Dinantian	43
	Appendix B: Quantitative petrography results	45

1 Introduction

1.1 Geothermal energy and the energy transition

The geothermal environment in the Netherlands is evolving quickly these days. Awareness grows and people notice the importance of the transition of energy generation from fossil fuels to more sustainable energy sources. The Paris Agreement from 2015 states that global warming should be limited, with a maximum of 2 degrees Celsius temperature increase and limiting CO₂-emissions. With the goal set by the Dutch government to be CO₂-neutral at the end of the year 2050, concrete measures are taken. Geothermal energy has been an ongoing debate in the Netherlands since 2007, when the first geothermal doublet was installed. By January 1, 2019, 24 doublets had been realized in the country, with growing numbers (Mijnlieff 2020).

Solar power and windmill parks are a solution to the generation and supply of sustainable energy. Geothermal energy, however, is currently solely used for greenhouse horticulture and heating homes. Due to usage of shallow aquifers, temperatures needed for energy generation (+120°C) are not reached. To reach such temperatures, drilling depths of >4km are required, assuming that we are confronted with a geothermal gradient of 30°C/km for the Dutch subsurface (Bonté et al. 2012). Porosity and permeability, which are important factors for the appliance of geothermal heat production, are very low at such great depths.

1.2 Potential of Dinantian carbonates in the Netherlands

Of all carbonate environments, dolomitized shelf facies are known to include important reservoirs and more hydrocarbons worldwide than any others, even at great depth (Macurda et al. 1997). Recent studies have looked at possibilities for ultra deep geothermal (UDG) in the Netherlands. EBN and TNO joined efforts and set up the SCAN program (Dutch abbr. for Seismic Campaign for Geothermal Energy Netherlands) at the beginning of 2019. This comprises a 3-year program, in which existing seismic data is used and re-processed to make an estimation of where the Dutch subsurface has potential for UDG. In the program there is an emphasis on certain areas with low data density. Examples of this are Dinantian carbonates in the northern Dutch onshore (Fig.1).

These carbonates are encountered over 4 km depth. Not many wells have been drilled into the Dinantian sequence, since most companies targeted the shallower Rotliegend interval due to interest in hydrocarbons. Only two wells fully penetrate this deeper Dinantian interval: Uithuizermeeden-02 (UHM-02) in Groningen in 2002 by NAM, and Luttelgeest-01 (LTG-01, see Fig.1 for location) in the Noord-Oost polder of the Flevoland province in 2004 by Total. The wells had been drilled to test the presence of hydrocarbons in the Dinantian carbonates, which were not encountered. Not much seismic data is available, but on the available profiles the shape and margins of a platform can clearly be observed. Bonté et al. (2012) found thermal anomalies in well LTG-01, with temperatures exceeding the normal geothermal gradient at depths greater than 4 km. Van Oversteeg et al. (2014) applied a Horner temperature correction to the well data to find a geothermal gradient of 45°C/km (Fig.2). Thus, if such a reservoir would be suitable for UDG, water with temperatures of 150 to 200°C could be produced, which are sufficient for electricity generation. However, as stated by previous authors (e.g. Reijmer et al. 2017; Mozafari et al. 2019), the carbonates are very tight due to their encountered depth, implying very low matrix porosity and permeability. Therefore, a deep carbonate reservoir is dependent on secondary permeability from karst, fractures and diagenetic features to make fluid flow possible.

In Californië, province of Limburg, Dinantian carbonates have already been subject to extraction of geothermal heat. In northern Belgium, saline aquifers in carbonates of Dinantian age are used for the production of geothermal energy (e.g. the Beerse-Merksplas doublet and the recent Balmatt project). The Heibaart dome in Loenhout, another Dinantian carbonate reservoir, is used for natural gas storage. These locations show the potential for the use of Dinantian carbonates as a reservoir for geothermal heat production. It should however be noted that these projects use Dinantian carbonates which are encountered at shallower depths (1 – 2.5km) and thus likely have a lower decrease in porosity and permeability, making it easier for fluid flow to occur.

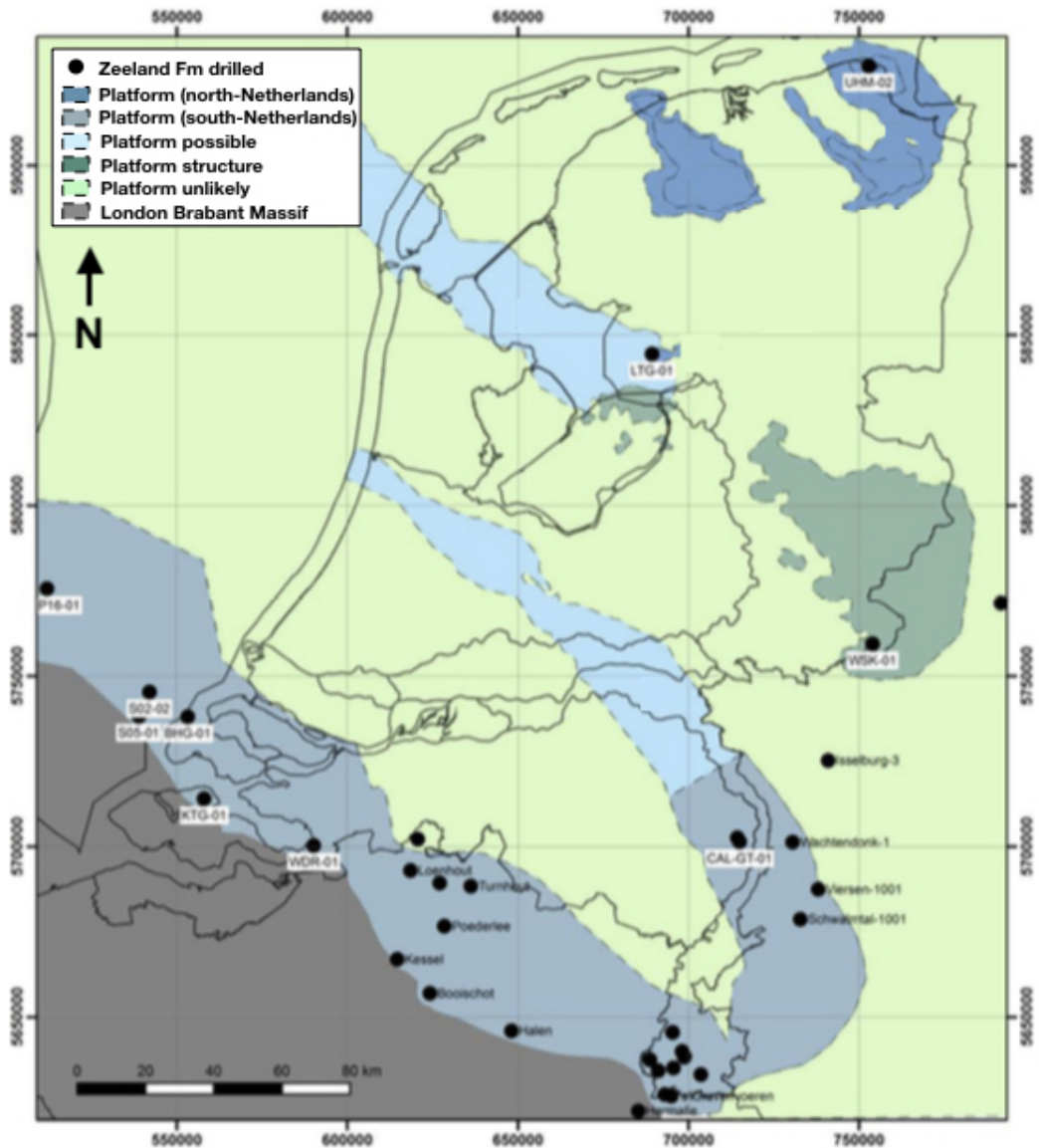


Figure 1: Distinction of Dinantian rocks in the Dutch subsurface and of neighbouring countries. Black dots show wells that reached or penetrated the Dinantian sequence. Modified after Boëem et al. (2016).

Other Dinantian platforms are the oil producing Tengiz and Kashagan fields in Kazakhstan (Weber et al. 2003; Ronchi et al. 2010). These reservoirs are found in Dinantian carbonate platforms and are also encountered at $\pm 4\text{-}5$ km depth. Diagenesis has played an important role in the porogenesis of the reservoir, so studies on these carbonates provide good analogues for the carbonate rocks which are subject of this study.

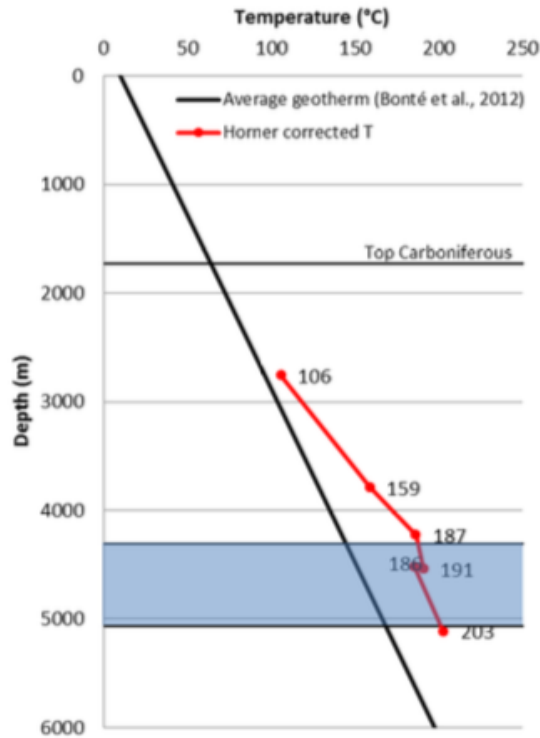


Figure 2: Graph with temperature versus depth, showing the average geothermal gradient for the Dutch subsurface (black line) and the Horner corrected temperatures for LTG-01 (red line). The depth of the interval of the Dinantian carbonates is indicated with the blue shaded area (Oversteeg et al. 2014).

1.3 Study objective

The scientific question to answer in this study is to be able to understand and quantify the flow properties distribution related to or influenced by diagenesis in deeply buried carbonate platform reservoirs, with a multi-scale (plugs, well and reservoir-scale) and multi-disciplinary (quantitative petrography, well log analysis and interpretation of seismic data) approach. By designing a workflow and applying it to reach the set objective on the Dinantian carbonates of the Luttelgeest platform, the Netherlands, the same could be applied on similar cases elsewhere. Next to that, the aim is to present a conceptual model for the specific case of the Luttelgeest platform to give an assessment on the geothermal potential of this carbonate reservoir.

The heterogeneity of carbonate reservoir properties remains a complex issue to tackle. This challenges the viability of geothermal projects. The strategy proposed and applied in this project is to infer, at multiple scales, those diagenetic phases that have significant influence on the potential fluid flow across the reservoir structure.

2 Geological Setting

2.1 Tectonic setting

2.1.1 Caledonian and Variscan orogeny

Two main orogenies define the geological history of the Netherlands and, on a larger scale, NW Europe: the Early Paleozoic Caledonian orogeny and the Late Paleozoic Variscan orogeny (Schulmann et al. 2014). The exact dating of both orogenies remains difficult, as they both comprise significant amounts of time, affecting different regions at different stages (Fig.3). The carbonate platform subject of this study is located within the North Western European Carboniferous Basin (Fig.4), which has a crystalline basement originating from the micro-continent Avalonia in relation to the Caledonian orogeny. This orogeny is generally referred to as the consolidation of Avalonia and Baltica, closing the Tornquist Sea during the Late Ordovician (Cocks & Torsvik 2005). The amalgamation of these micro-continents was followed by the closing of the Iapetus Ocean and the collision with Laurentia during the Silurian period. This resulted in the formation of the continent commonly known as Laurussia or the Old Red Continent, establishing the Caledonian orogenic cycle which eventually ended in the Early Devonian (Kombrink 2008). The Caledonian orogeny was followed by the Variscan orogeny from the Early Devonian onwards. The Variscan orogeny is mainly characterized by the closure of the Rheic Ocean due to the collision of Gondwana (and its derived micro-continents) and Laurussia. This collision created the supercontinent Pangaea and with it a suture zone referred to as the Variscan front. Consequently, the Rheohercynian Zone was formed as a result from the closing of the Rheic Ocean (Kombrink 2008).

2.1.2 Devonian

From Early Paleozoic up and until Early Devonian, little is known in the northern Netherlands onshore area. In Dutch lithostratigraphy, Lower Devonian is absent (Geluk et al. 2007). From analogues and data from other areas it is believed that from the Early Devonian, a back arc extension resulted in a rifting phase that created the opening of the Rheohercynian rift basin (Ziegler 1990). This occurred along the southern margins of the Old Red Continent and it created an extensional regime that resulted in fault bounded half-grabens with NW-SE and NE-SW strike (Fig.5; De Jager 2007; Kombrink 2008; Van Hulten 2012). The Rheohercynian rift basin was infilled by sediments that were sourced from its northern and southern margins; the Old Red Continent and the German Crystalline High respectively (Kombrink 2008; Reijmer et al. 2017). The created basin from Early Devonian times started to close in the Middle Devonian during a small period of SE directed subduction (Franke 2000). Back-arc extension again took over in the Late Devonian for a short phase which was followed by another period of compression known as the Bretonian orogenic pulse at the transition into the Carboniferous.

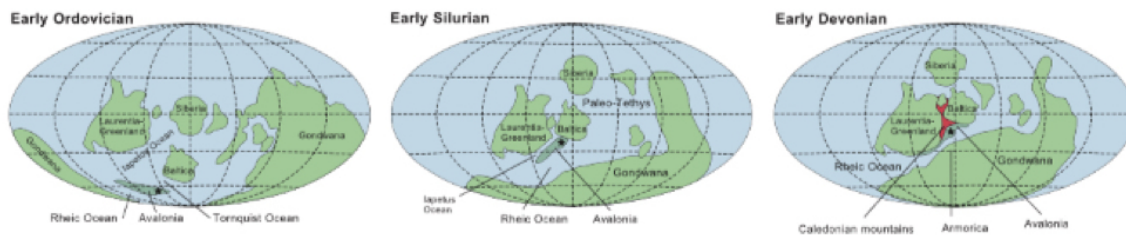


Figure 3: Reconstruction of plate tectonics, illustrating the northward movement of Avalonia and its collision with the land masses of Baltica and Laurentia, creating the Caledonian mountains. The black star roughly indicates the paleo-position of the study area (Geluk et al. 2007).

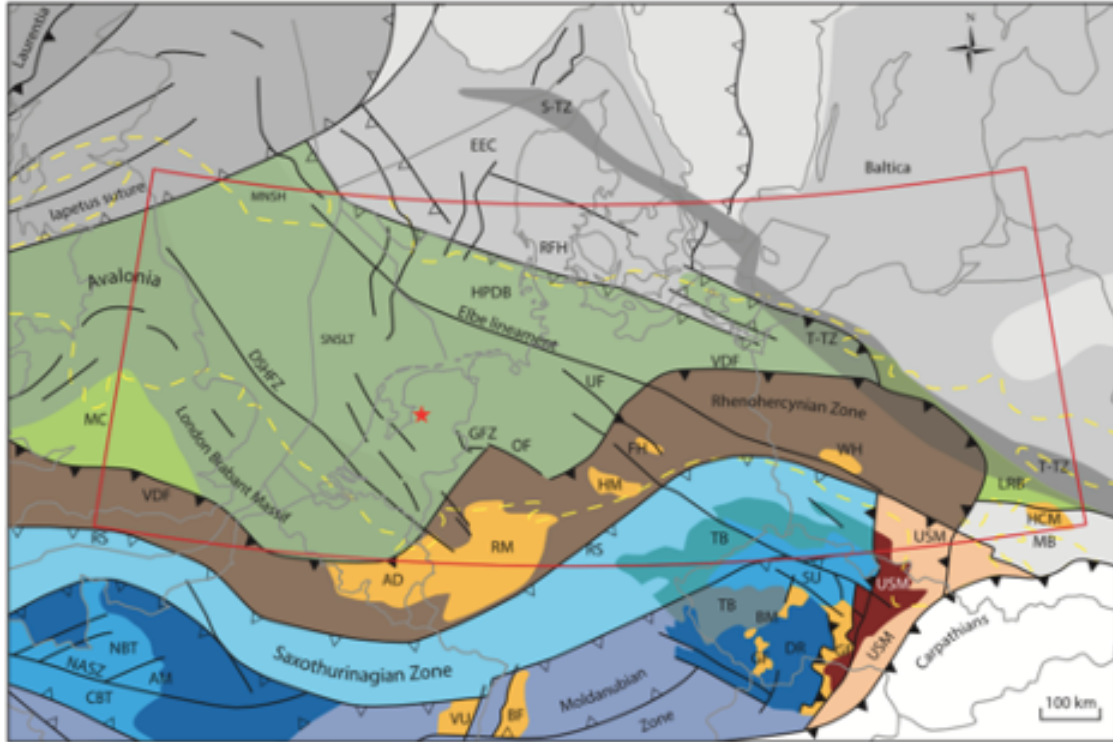


Figure 4: Structural elements of the NWECEB. The dark grey and light grey areas represent Laurentia and Baltica, respectively. The green area indicates the Avalonian microcontinent. The Rhenohercynian Zone is shown in brown and represents the fold and thrust belt originating from the Variscan orogen. The microcontinents that were accreted during the Variscan orogen are shown in dark and light blue. Red star indicates the position of LTG-01 and the yellow dashed line indicates the extent of Carboniferous rocks in the Southern Permian Basin area. Oceanic sutures are indicated by open ticks and orogenic frontal zones are indicated by filled ticks.

Key: Post-Palaeozoic platforms: MNSH: Mid North Sea High, RFH: Ringkøbing-Fyn High. Postulated Palaeozoic terranes and possible terrane/sub-terrane boundaries: CBT: Central Brittany Terrane, DSHFZ: Dowsing-South Hewett Fault Zone and continuation in Roer Valley Graben (SE), GFZ: Gronau Fault Zone, OF: Osning Fault Zone, RS: Rhenohercynian Suture Zone, SNSLT: Southern North Sea Lüneburg Terrane, LRB: Lisogóry-Radom Block, MB: Malopolska Block, UF: Uelzen Fault. Proterozoic-Palaeozoic tectonic elements: AD: Ardennes, AM: Armorican Massif, BF: Black Forest, BM: Bohemian Massif, DR: Drosendorf Unit, EEC: East European Craton, GF: Gföhl Unit, HCM: Holy Cross Mountains, HM: Harz Mountains, MC: Midland Craton, NBT: North-Brittany Terrane, RM: Rhenish Mountains, S-TZ: Sorgenfrei-Tornquist Zone, SU: Sudetes Mountains, TB: Tepla-Barrandian Basin, T-TZ: Teisseyre-Tornquist Zone, USM: Upper Silesian Massif, VDF: Variscan Deformation Front, VU: Vosges Unit, WH: Wolsztyn High. Map from Kombrink (2008), mainly based on Pharaoh (1999) with modifications using Drozdowski et al. (2005), Narkiewicz (2007) and Ziegler (1990).

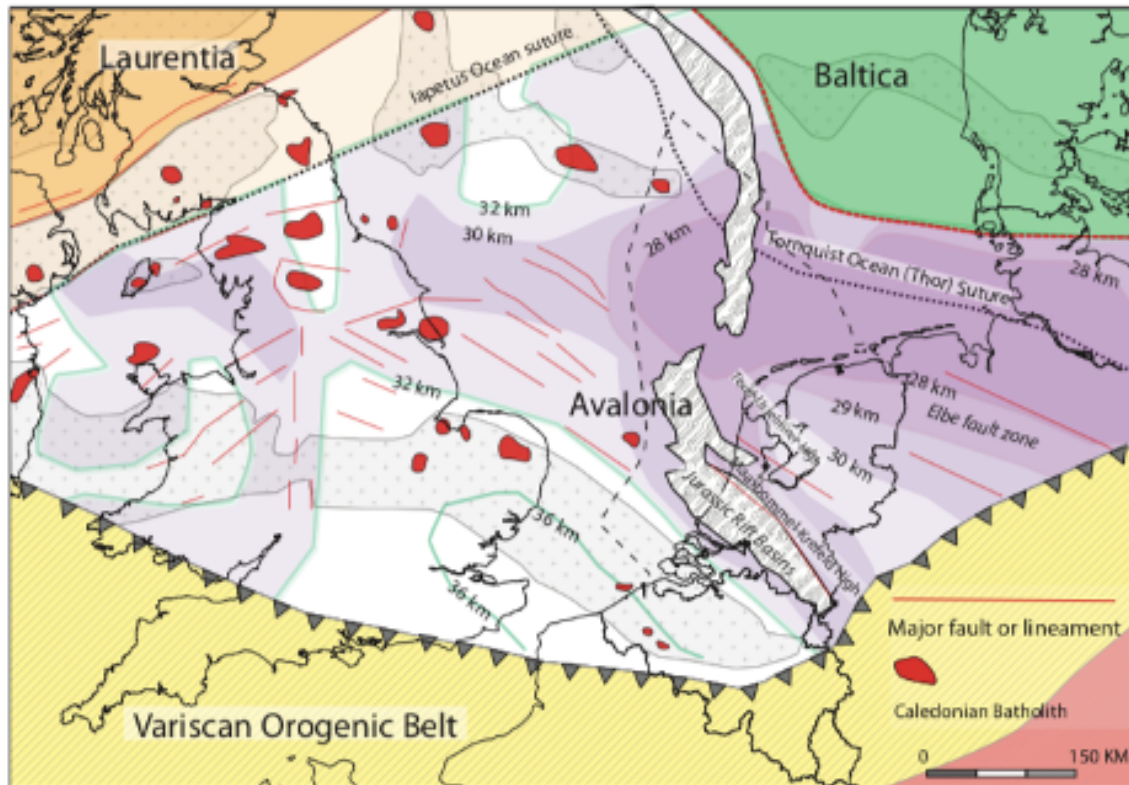


Figure 5: The depositional basement of the NWECEB is formed during the Silurian as part of the Caledonian triple continental plate collision of Avalonia (purple), Baltica (green) and Laurussia (orange). Structural elements with major faults and lineaments are indicated and show NW-SE to NE-SW strike. Grey highlighted areas show the later location of Jurassic rift basins (Van Hulten 2012).

2.1.3 Early Carboniferous (Dinantian)

During the first two stages of the Carboniferous (Tournaisian and Viséan), another phase of extension preceded the final closure of the Rhenohercynian Zone in the late Early Viséan (Ziegler 1990; Franke 2000; Kombrink 2008). The rifting phase ensued in the reactivation of features of structural weakness in Caledonian structures. It created a major tilted fault block system (Fig.6), which is believed to still control the structural style of large basins and orogens from later times, such as the NWECEB (Hornveld 2013 and references therein). The tilted fault block system that originated from the reactivation of weak Caledonian structures created heavily asymmetric half-graben structures in which the footwall highs were a good place for carbonate build-ups to develop. Hanging wall blocks were filled by deep water deposits (Fig.7; Geluk et al. 2007). For NW Europe, the London Brabant Massif (LBM) acted as a relatively immobile and stable feature in the south of the NWECEB and a spot for these carbonate platforms to flourish. Post-Carboniferous Namurian shale deposits overlap these platform structures (Fig.8) and are believed to have provided charge of hydrocarbons into the carbonate limestones (Van Hulten & Poty 2008; Reijmer et al. 2017). Through time in NW Europe, the strike of faulting changed. The extension in the Early Tournaisian started with N-S extension in northern England (Fig.5), slowly moving south-east with a more NW-SE strike (Fraser & Gawthorpe 1990; Coward 1993). In the Campine basin in Belgium, comparable fault block structures have been observed, although hanging wall basins do not show deep water facies (Muechez et al. 1991; Kombrink 2008).

The north-west of Europe was mainly characterized by the development of carbonate platforms (both marginal and isolated) and deposition of marine shales and chert layers in areas of low clastic input (Bless et al. 1976; Cameron 1992; Schroot et al. 2006). Areas proximal to more clastic

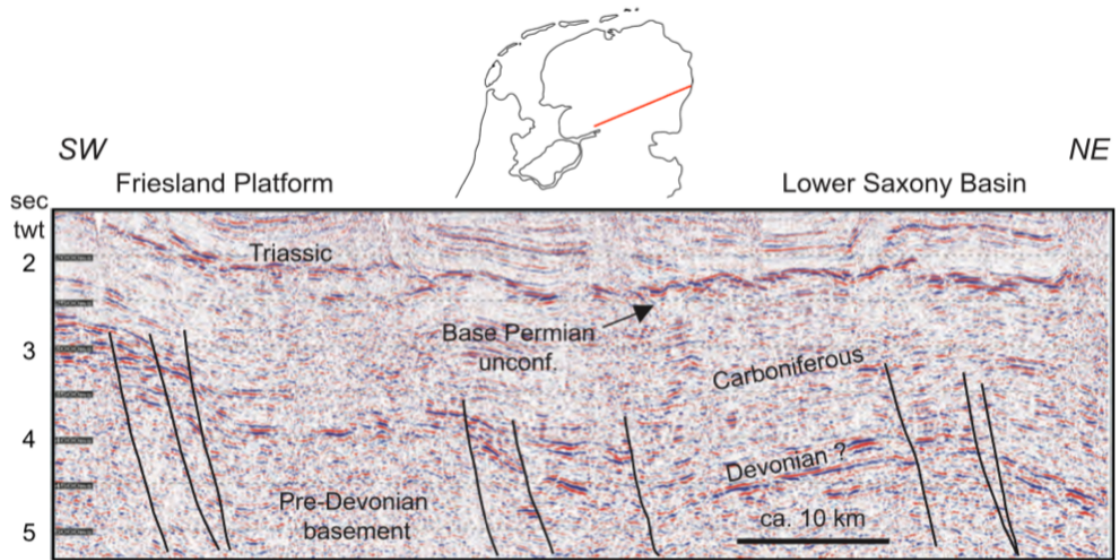


Figure 6: Deep seismic line across the north-eastern Netherlands. Top map shows location of the seismic line. A tilted fault block system is clearly visible in pre-Carboniferous sediments. Modified after De Jager (2007).

sources show more deltaic and turbidite facies. Platforms at the foot walls just north of the LBM were frequently exhumed and reburied, exposing them to the surface which made them subject to karstification (Reijmer et al. 2017; Broothaers et al. 2019). The platforms in the north of the Netherlands remained buried, not subjected to meteoric karstification. In the Early Visean the Rhenohercynian Zone closed, coinciding with extensive thrusting (Van Adrichem Boogaert & Kouwe 1997) and the platforms drowned following a sea level rise at the end of the Visean (Reijmer et al. 2017).

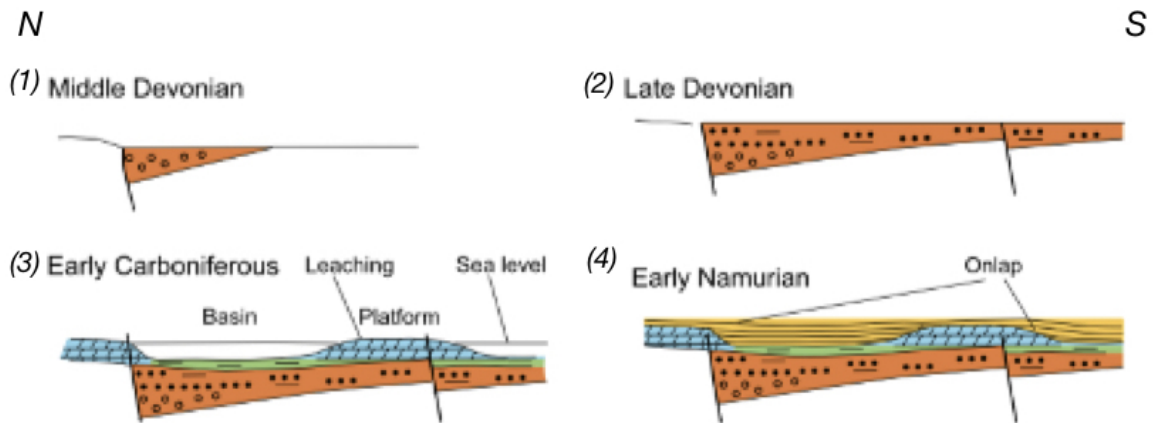


Figure 7: Schematic model for the phases of deposition of the Devonian and Lower Carboniferous in the area just north of the LBM. (1) & (2) Half-grabens controlled the sedimentation during the Middle Devonian to Late Devonian. (3) Extension continues and Dinantian carbonate platforms form on the footwall blocks while the hanging wall blocks are characterized by basinal deposits. (4) The Namurian transgression progressively buried and killed the platforms and their topography (De Jager et al. 2007).

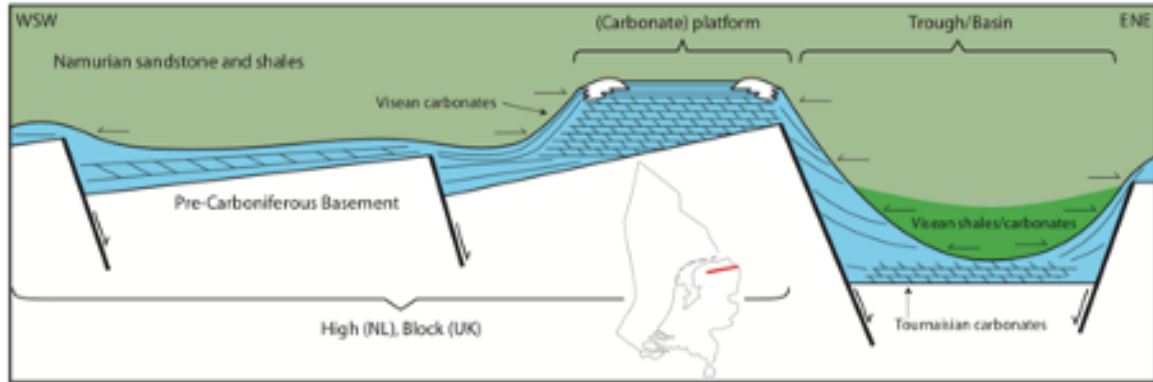


Figure 8: *Schematic cross section of the interpretation of the line shown on the small map of the Netherlands. Dinantian sequence is shown in light blue, Namurian onlapping shales in green (Kombrink 2008).*

2.1.4 Late Carboniferous (Silesian)

The first stage of the Silesian (the Namurian) was characterized by a phase of subsidence controlled by thrust loading (Kombrink 2008). NW Europe ensued into a sag phase and rift structures were covered by deep sea and deltaic facies. With the major part of the basin geographically remote from deltaic influxes, anoxic bottom conditions dominated which resulted in the deposition of low-permeable shales and chert layers onto the Dinantian sediments (Cameron and Ziegler 1997; Fig.7). Schroot et al. (2006) found similar facies at the top of the Dinantian sequence in the Southern North Sea. They also found evidence for other tectonic events affecting the area. Through seismic data interpretation, an intra-Namurian angular unconformity was demonstrated, implying either erosional truncation or onlap on that surface. Kombrink (2008) showed that Namurian shales are not present in some locations and here Westphalian rocks directly overlie the Visean carbonates. Also, Sissingh (2004) found evidence of Namurian volcanism in well NAG-01 in the Netherlands. Combining evidence, the previously suggested simple sag model appears to be too simple and large-scale tectonics during the Namurian must be considered.

The thermal subsidence continued in the second stage of the Silesian. During the mid-Westphalian, Variscan orogeny rose and created a N-S compressional tectonic regime. This event created relative uplift and a large regression in the NWECEB. The Variscan deformation front was migrating northwards, closing the back-arc seaway from the Caledonian back-arc extensional phase (Besly 1998; Schroot et al. 2006). In the western part of the NWECEB, fluvial deposits and red-bed formations were starting to form. These red-bed formations are characterized by reddened, bioturbated lacustrine deposits, paleosol-dominated overbank deposits and alluvial channel systems. By the end of the Westphalian, the whole area was covered with red-beds (Kombrink 2008).

The Stephanian (the latest Silesian stage) sediments overlie the Westphalian sediments unconformably in the east of the Netherlands and Germany (Ziegler 1990). Further uplift in the Stephanian reactivated the existing Caledonian NW-SE fault structures that were already established and, with that, the overlying sediments. Along these structures, sets of NE-SW to NNE-SSW faults were formed (Ziegler 1990). However, this stage is characterized by dextral and sinistral strike-slip faulting, resulting in sets of pull-apart basins. These ‘wrench faults’ were associated with thermal uplift into the Early Permian due to both intrusive and extrusive magmatism (De Jager 2007). This uplift likely caused erosion, implying that the Stephanian sediments had a much wider distribution than what can be deduced by wells and seismic data.

2.1.5 Permian

After the Variscan orogeny ceased by the end of the Westphalian, structures of the Carboniferous were still affected by wrench faulting and thermal uplift in the Early Permian. This structural deformation of the Carboniferous carbonates are argued to postdate Variscan movements (Geluk 2007). Lower Permian sediments are scarce in Europe and even absent in the Netherlands as the

end of the orogeny was characterized by non-deposition and erosion. The series of unconformities that were created in multiple areas in NW Europe were named together as the ‘Base Permian Unconformity’ (Geluk 2007). The unconformity represents a hiatus of 40 to 60 Ma at most places. Sediments from the early Middle Permian, known as Lower Rotliegend group, are found only locally and are of clastic and volcanic origin. The stratigraphy from Middle to Upper Permian is represented by the fluvial and eolian Upper Rotliegend group and the carbonate and evaporitic Zechstein groups. The combination of the sandy Rotliegend and the Zechstein salt is well known for hydrocarbon exploration in the Netherlands, with 95% of their large reserves found in these rocks. The end of the Permian was characterized by thermal subsidence throughout the whole area, leading to the formation of the Northern and Southern Permian basins (Geluk 2007).

2.1.6 Mesozoic

Thermal subsidence continued into the Triassic and eventually turned into the breakup of supercontinent Pangaea during the Kimmeridgian rifting phase. This started in the North-Atlantic, between Greenland and Scandinavia. The rift propagated southward in direction of the Central Atlantic Ocean and reached the Southern North Sea in Middle Triassic times. Although rifting was oriented mostly E-W, created Mesozoic basins in NW Europe had a more NW-SE orientation (De Jager 2007). As mentioned before, it is believed that this NW-SE orientated extension occurred due to pre-existing Caledonian basement structural elements that were reactivated and propagated into younger sediments.

The Jurassic period comprises a second phase of the break-up of Pangaea into the Central Atlantic Ocean and Gondwana, which was separated from Laurussia. Rifting in NW Europe continued and the northern and southern Permian basins were split into multiple smaller basins. The Netherlands Central Basin was created in this period and is currently the largest geothermal play in the country (Mijnlieff 2020). Rifting ceased in the Early Cretaceous and fault activity stopped and in Middle Cretaceous, another period of thermal sag started. Transgression occurred on large scale in NW Europe, drowning most basins and in the Netherlands the coastline shifted to the Friesland platform. The end of the Cretaceous was defined by tectonic activity due to the Alpine orogeny and the uplift of basins in the northern foreland, resulting in truncations of Upper Cretaceous and older sediments (Van Adrichem-Boogaert & Kouwe 1997; De Jager 2007).

2.1.7 Cenozoic

Due to the northward movement of the African-Arabian plate, which was the onset of the Alpine orogeny, large parts of NW Europe were inverted and subjected to uplift. This resulted in erosion and depositional thinning of Cretaceous sediments, as well as local truncation of older sediments. De Jager (2007) studied the Cretaceous-Tertiary successions on the basin flanks and found that uplift was a continuous process. This process ceased by the end of the Paleogene, when thermal sag accompanied with a sea level rise occurred in the Southern North Sea. The latest inversion, during the Oligocene, is poorly developed in the Dutch area, yet more evident towards the UK (De Jager 2007).

2.2 Stratigraphic distribution of the Dinantian in the Dutch subsurface

Pre-Silesian sediments in the Dutch subsurface are found at considerably variable depths. In the province of Limburg (SE) Dinantian rocks are found at outcrops at the surface, but also expected to be buried to over 10 km depth in the offshore subsurface. Below the Dinantian, minorly deformed Devonian sediments are encountered. These overlay a metamorphic Caledonian basement. Since wells in the Netherlands have reached the Silurian at max, this is based on wells in Belgium (Geluk et al. 2007). The Devonian sediments are grouped into two units: the Old Red group and the Banjaard group. In the Dinantian sequence, a division is made between clastic sediments (Farne group) and carbonate sediments (Lower Carboniferous group). Fig.9 shows a schematic overview of the pre-Silesian stratigraphy. See Appendix A for a detailed description of the different sedimentary groups and units.

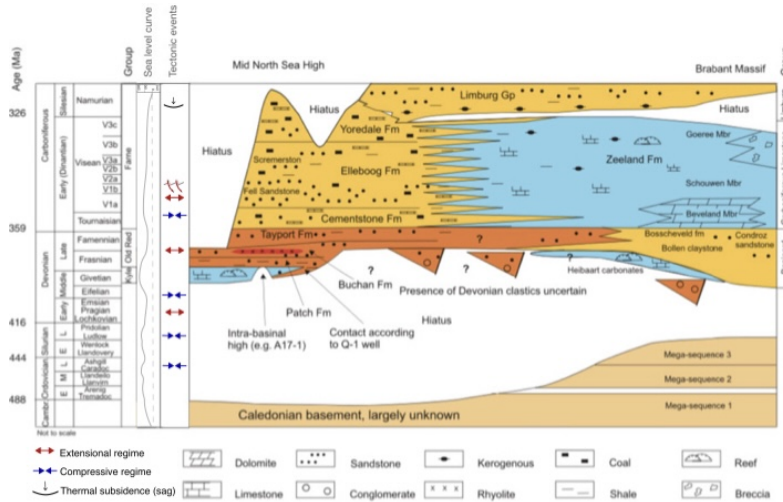


Figure 9: Schematic stratigraphic overview of the pre-Silesian deposits in the Netherlands and surrounding areas. Stratigraphy is mainly based on available well data (from the Mid North Sea High and the Brabant Massif). The area inbetween has been interpreted and is highly speculative. For elaboration of members, see Appendix A (modified after Geluk et al. 2007, sea level curve after Haq & Schutter 2008).

Chronostratigraphically, the Dinantian can be subdivided in three units based on their age: Tournaisian, Late Chadian-Arundian and Holkerian-Asbian-Brigantian. The transgression in units can be observed from the carbonitw deposits of the Zeeland Formation in the south to the more clastic deposits in the north (Yoredale, Elleboog, and Cementstone Formations). The Tournaisian interval is often poorly developed or fully missing. Late Tournaisian to mid Viséan carbonate ramps developed along the northern margin of the London-Brabant Massif, in the southern Netherlands (Mozafari et al. 2019). In the Dutch wells LTG-01 and UHM-02, the Tournaisian is not present (Fig.10).

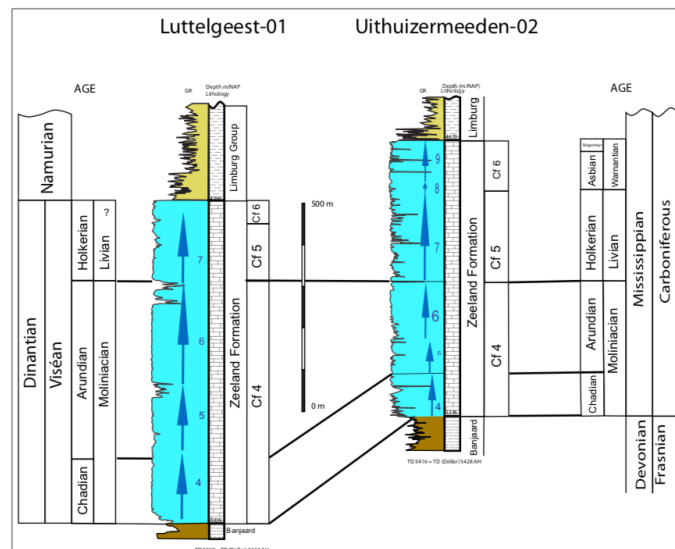


Figure 10: Cross section showing a stratigraphic comparison between the LTG-01 and UHM-02 wells. The Gamma Ray (GR) log of both wells is shown for comparison. Both wells reached TD (Total Depth) in the top of the Famennian clastics. The arrows show widely recognized 3rd order sequences (Poty et al. 2002). The age interpretation is based on foraminifera (Cf zones). Contrary to the UHM-02 well, the reef growth in LTG-01 was terminated before the end of the Viséan (Van Hulst 2012).

2.3 The Luttelgeest platform

The Luttelgeest platform, subject of this study, is a carbonate platform situated in the Dutch subsurface at the position of the Noord-Oost polder in the province of Flevoland. The platform spans a depth interval of 4355 to 5123 m, therewith reaching a thickness of 768 m. It has an elongated shape with E-W orientation and dimensions of ± 14 km E-W and ± 8 km N-S (Fig.11; Lipsey et al. 2016). Thermal analyses have shown that a temperature anomaly exists in the subsurface, and temperatures of 160 °C at 4 km depth and even over 200 °C at 5 km depth are reached (Oversteeg et al. 2014; Lipsey et al. 2016). Due to the great depth at which the platform is encountered, the rock matrix has a very low permeability but studies have shown that it hosts multiple fracture systems (Lipsey et al. 2016; Mozafari et al. 2019). In the south, the platform is bounded by a steep fault system, while the northern margin gradually transitions into the Friesland platform.

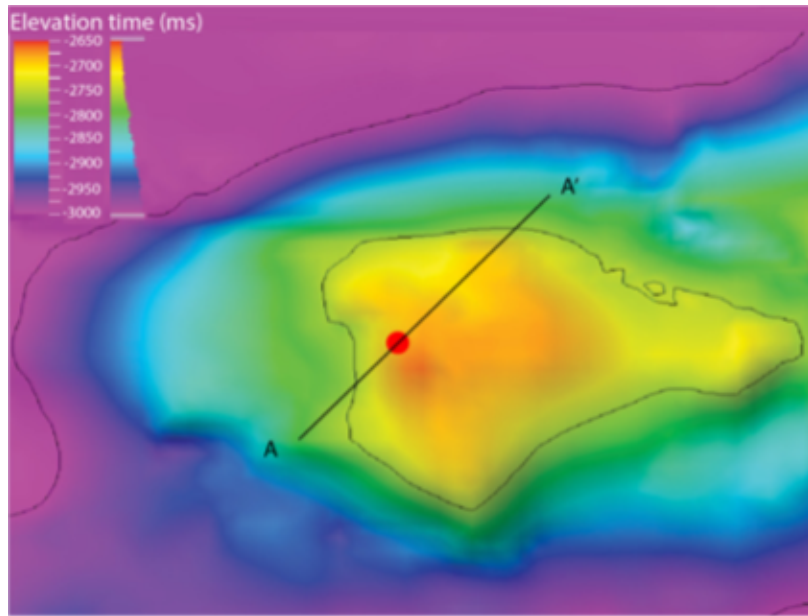


Figure 11: Subsurface top view of the Luttelgeest platform. Line A-A' indicates location of the SW-NE seismic line from Fig.20. The location of well LTG-01 is shown with the red dot (Lipsey et al. 2016).

3 Data and Methodologies

3.1 Literature study on available datasets

For studies on the Luttelgeest platform cores, thin sections, photomicrographs and well logs were made available by the Geological Survey of the Netherlands (part of TNO). Only one well, Luttelgeest-01 (LTG-01), penetrated the Dinantian interval. Parts of the data sets have been analysed and interpreted in multiple studies (see Kombrink 2008; Van Hulst 2008, 2010, 2012; Lipsey et al. 2016; Reijmer et al. 2017; Mozafari et al. 2019; SCAN Project). These studies have been thoroughly analysed to create a synthesis of results from previous work.

3.2 Quantitative petrography

Two short cores of LTG-01 were slabbed from the Dinantian interval, with a total length of 5.5 m. Core 1 is taken from 4378.5 to 4376 m depth and core 2 from 4473 to 4470 m depth. The cores are stored in the core house storage of TNO in Zeist (NL). Quantitative petrography was carried out to quantify different minerals and cements and their corresponding diagenetic phases. This could indicate levels of diagenesis in certain areas of the reservoir rock which can be linked to their influence on the potential fluid flow properties. The quantification is done by point counting on scans and photomicrographs of thin sections that were taken from the core and cuttings at multiple depths. 25 thin sections were taken from the core and the cuttings (Table 1) and were scanned using a flatbed scanner, at 2400 dpi. The point counting was carried out using the software JMicroVision (v. 1.3.3) with n=150 points per sample.

Firstly, a classical petrographic analysis was carried out to distinguish different minerals and classify types of cement that resulted from different diagenetic phases. Mozafari et al. (2019) did a petrographic analysis, from which will be built on in this study. Also, the relative timing of cementation is a key interpretation for the study. This was done on photomicrographs of the thin sections.

Second, a distinction was made between matrix and veins (partially cemented fractures) within the thin sections, as the matrix of the rock is known to have a very low porosity (close to 0%) and fluid flow is expected to occur through fractures and veins (Lipsey et al. 2016; Reijmer et al. 2017; Mozafari et al. 2019). Thin sections containing veins (5 pcs) were selected. Subsequently, point counting was carried out to quantify the volumetric percentage of veins in the host rock.

Next, photomicrographs of parts of veins were subjected to point counting to quantify overall mineral and (intracrystalline) porosity percentages in the veins. The veins host multiple cements of different diagenetic phases and can thus give a clear quantification of these phases.

Lastly, point counting on cuttings (16 pcs) was carried out. A distinction was made between calcite, dolomite, quartz and opaque minerals. The calcite/dolomite ratio is deemed important because that could indicate a level of diagenesis of the rock. In previous work, dolomite-rich horizons were suggested to have better flow properties due to higher fracture density (Leverink & Geel 2019). Quartz is argued to be in situ infill of vugs and cavities during deposition (Mozafari et al. 2019). Opaque minerals could indicate precipitation from hydrothermal fluids.

Thin sections	Cuttings	
4376.18	4400	4856
4376.84	4426	4902
4377.40	4520	4946
4377.70	4570	5010
4470.30	4600	5052
4470.63	4650	5066
4471.92	4768	5076
4472.02	4800	5082
4472.48		

Table 1: *Depths (m) of thin sections and cuttings taken from the core of LTG-01.*

3.3 Seismic interpretation, facies associations and well log integration

With a standard seismic approach, key seismic horizons were defined from two representative 2D seismic reflection profiles. Seismic interpretation was performed using Petrel 2019 software (v. 10.0.18362). The 2D seismic data, shot by NAM, is openly available at the NLOG website. The two seismic lines (803006 and 803007) that are used in this study show a good representation of the shape of the platform. Unconformities and stratigraphic surface geometries such as onlap and offlap are found to construct stratigraphic sequences. Faults and geological structures are mapped. Analysis of seismic facies within the selected seismic packages was performed using reflection configurations and properties (amplitude, internal geometries, continuity and terminations), a technique applied in other studies (e.g. Papadimitriou et al. 2018). With each configuration, different possible depositional environments can be attributed. The derived seismic facies are then coupled to the interpreted stratigraphic boundaries and well data. Laterally, different facies can exist and affect reservoir properties of the rock. Interiors of carbonate buildups show low amplitude reflectors due to the lack of continuous horizons in it (Macurda et al. 1997). Therefore, integration with structural

geology and well logs is needed to get a clear view on the structure of the buildup, the attribution of depositional environments and reservoir properties that are related to that. The FMI of LTG-01 consists of oriented high-resolution, 240 trace resistivity data and is openly available on the NLOG-website.

4 Synthesis of Previous Work

4.1 Introduction

Well Luttelgeest-01 (LTG-01) is located in the North Central Netherlands (Fig.1). Drilling was done by Total, with exploration purposes. It started on May 26, 2004 and the well was abandoned on March 8, 2005, with only minor gas shows (Boxem et al. 2016). The well reached a depth of 5162 m. The Dinantian interval starts at a depth of 4355 m and has its base at 5123 m depth. This thick Viséan section of 768 m was encountered overlying the Devonian Banjaard Group, which the well just reached into and has been interpreted as a carbonate platform (Kombrink 2008; Van Hulten & Poty 2008, 2009). The information spread out in this chapter is synthesized and based on thorough literature review. A detailed study and data analysis on LTG-01 has been performed by Energie Beheer Nederland (EBN) during the SCAN project (Dutch abbreviation for Netherlands Seismic Campaign for Geothermal Energy). This work is published in a report by Mozafari et al. (2019). A fracture characterization analysis was also performed by Panterra, which was published in a report by Van Leverink & Geel (2019).

4.2 Sedimentology

Cores and cuttings of LTG-01 have been studied to differentiate sedimentary depositional environments by Mozafari et al. (2019). The created sedimentary logs are shown in Fig.12. The cores are dominated by bioclastic peloidal packstones and grainstones and crinoids, fragments of echinoids, calcareous algae, foraminifera and brachiopods were encountered. Locally, bioclasts are aligned, indicating a high energetic depositional environment in shallow water settings, above wave base. The larger part of the cuttings consist of grain-supported, high energy facies. Intraclasts and ooids are common, suggesting a continuous high energetic environment. The microbial nature of many of the cuttings suggest very shallow conditions, and fenestral textures may indicate short-lived exposure (intertidal settings). Siliciclastic cuttings are present but are likely to represent vug infill. Dolomite is rare throughout the well except for the base of the well (5000 to 5120 m depth). Analyses of cuttings suggest that the lithology at this depth is a dolomitic limestone, rather than pure dolomite. The high API-peaks seen in the gamma ray tool represent Uranium peaks, and do not show any clay content (no Potassium from the spectral GR log). It is possible that the higher Uranium peaks represent calcrete intervals at cycle tops (Mozafari et al. 2019).

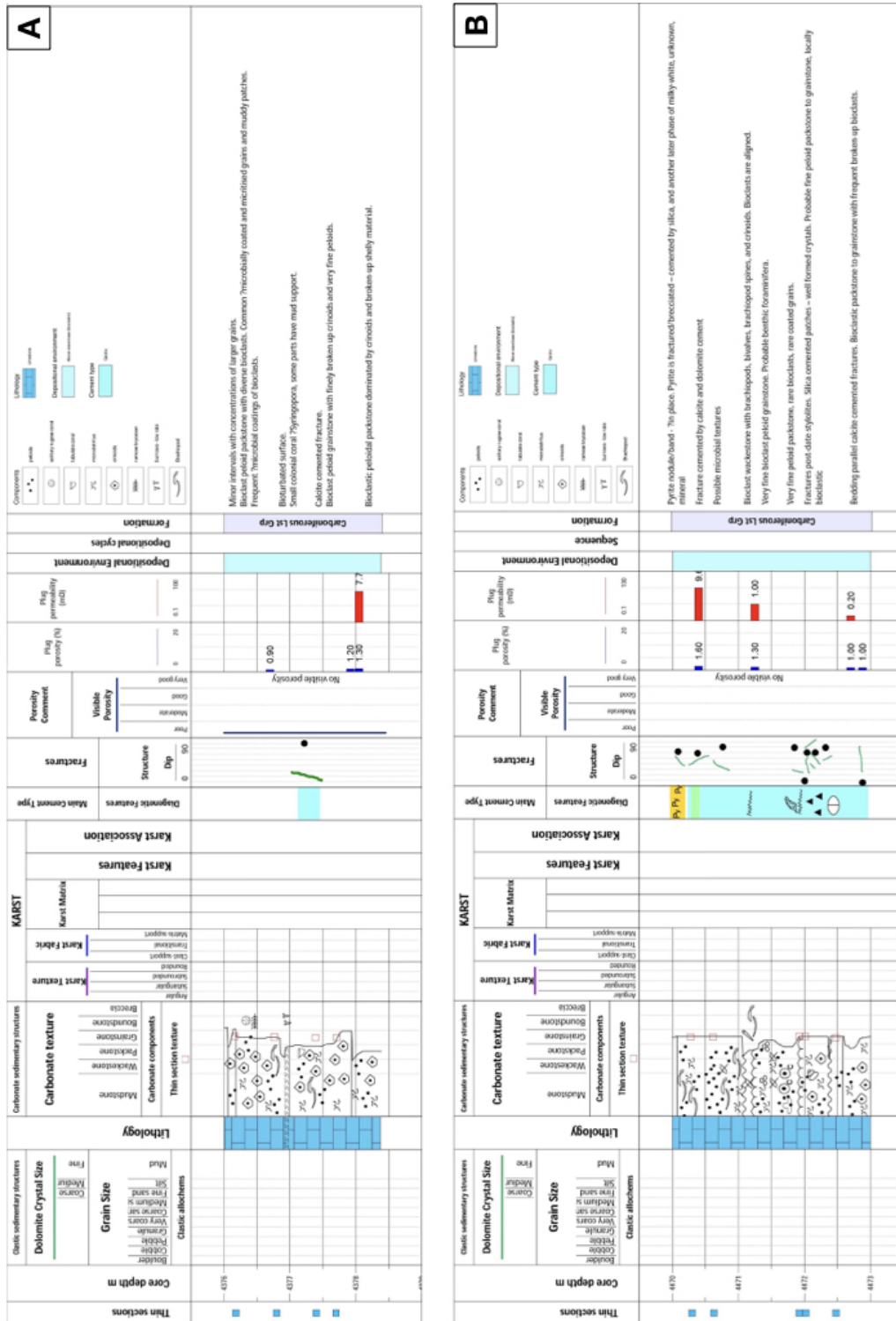


Figure 12: Sedimentary logs of slabbed cores. (A) core 1, depth: 4378.5 to 4376 m, (B) core 2, depth: 4473 to 4470 m. Logs are from SCAN Project.

4.3 Sequence stratigraphy

The basal Dinantian sedimentary sequences from the Tournaisian are missing in the Luttelgeest platform. This absence has been interpreted as a result of onlap on a structural high. Seismic data in the study area are very poor, so cycles have been established by correlation with well UHM-02 (Fig.13) and other cores that drilled the Dutch Dinantian interval. As such, the following cycles have been recognized from base to top (Mozafari et al. 2019):

Cycle 1c: This cycle represents the initial onlap of the basement high and is probably incomplete. The subtidal facies are dominated by oncoids and highly micritized grains (observed in well S02-02), which suggest that deposition took place in a restricted shallow carbonate ramp setting.

Cycle 1d: This cycle shows a thin, moderate gamma ray value TST followed by a low gamma ray HST. It consists of fine, well sorted bioclastic pack-grainstones (from well S05-01) deposited on a high energy platform interior depositional setting.

Cycle 2a: This cycle shows a thick, moderate gamma ray value TST followed by a low gamma ray HST. In well S05-01 it consists of medium- to thickly-bedded, bioclastic pack-grainstones and is interpreted as a high energy platform interior depositional setting.

Cycle 2b: This cycle shows a thick, high gamma ray value TST to maximum flooding, suggesting a period of drowning followed by a thick, very clean gamma ray HST. It consists of medium-bedded bioclastic grainstone/packstone with some coated and micritised grains (from well S05-01) interpreted as a high energy setting above normal wave base, in an inner carbonate ramp to shelf setting.

Cycle 2c: This cycle is a thin depositional cycle, mainly showing a high gamma ray value TST and maximum flooding followed by a thin, moderate gamma ray HST. It was cored in well S05-01 where it consists of medium-bedded bioclastic grain-packstone with some coated and micritised grains. There is no indication of emergence within the core. This suggests a low to moderate energy platform interior depositional setting.

Cycle 2d: This cycle shows a thick, high gamma ray value TST and maximum flooding interpreted as a drowning event followed by thick clean gamma ray value HST. It consists of medium- to thickly-bedded bioclastic peloidal pack-grainstones and is interpreted as a high energy aggradational platform interior depositional setting.

Cycle 3a: This is the only cycle recorded in cores of LTG-01. It mainly consists of bioclastic peloidal packstones and grainstones, ooids indicate a high energy platform interior setting. At least one flooding event may be present. Common gamma spikes are interpreted as common karst cavities infilled by mudstone, but these were not observed in the two cores.

Cycle 3b: This cycle is observed in UHM-02 but is missing in LTG-01. In UHM-02 it has been interpreted as a high energy carbonate platform interior depositional setting. It shows muddy infills of karst cavities, which makes the gamma signature generally erratic, in which the gamma ray spikes are interpreted as these infills.

The overall setting of the cycles indicates deposition in a high energy platform interior setting. The emergence from cycle 2a to 2b shows a slight change from inner ramp to a more marginal setting, this is mainly based on observations in other wells. Cycle 2c is the only cycle that has indications of a lower energetic depositional setting, creating its sequence boundary with cycles 2b and 2d.

The part of the platform that is intersected by LTG-01 is Moliniacian to Livian in age, which describe the first two divisions of the Viséan. This suggests that the top of the Viséan (Asbian to Brigantian) is missing. However, as observed in seismic data, the well penetrates the platform through its margins and may therefore have missed the top layers. It is thus possible that the well missed the location of the sediments of cycle 3b (which are observed in UHM-02) or it suggests that the platform was already drowned before or during the Asbian (Fig.14; Mozafari et al. 2019).

4.4 Diagenesis and fracture analysis

With a total of ± 5.5 m of slabbed core, diagenetic features from the core do not show a good representation of the diagenetic history of the whole platform. However, cuttings from multiple depths through the whole platform have been retrieved and were studied for diagenetic features.

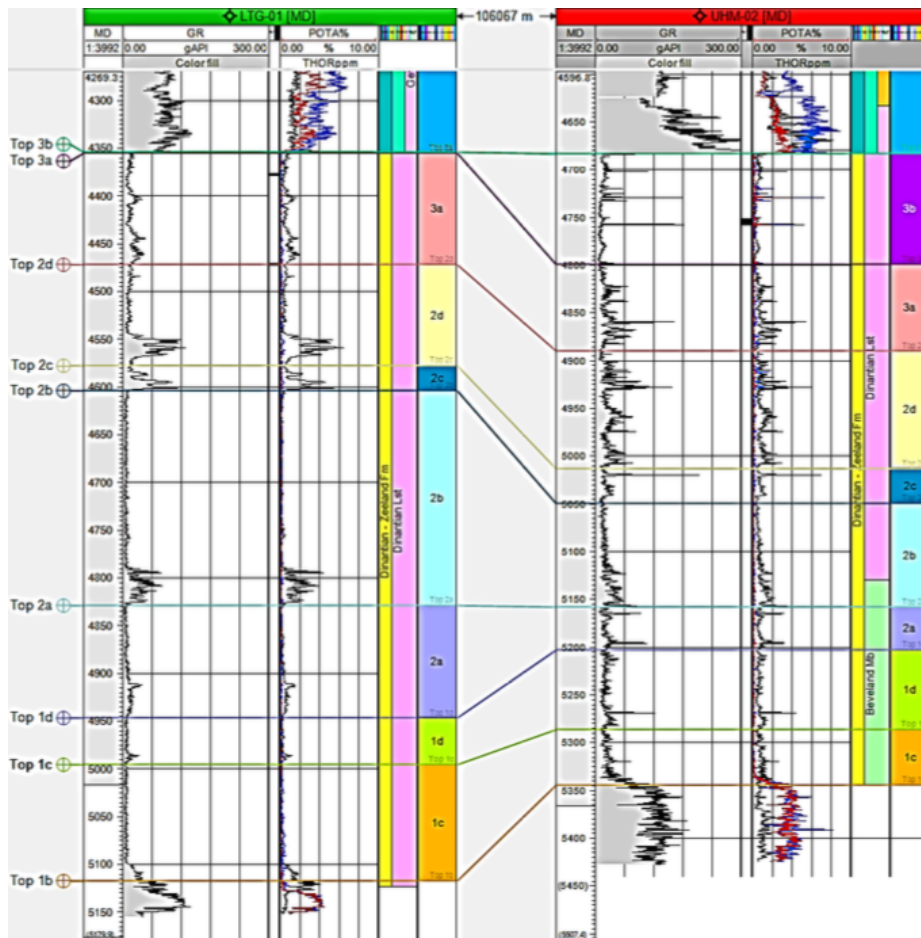


Figure 13: Correlation between the LTG-01 and UHM-02 wells, with the constituted sedimentary sequence cycles (Mozafari et al. 2019).

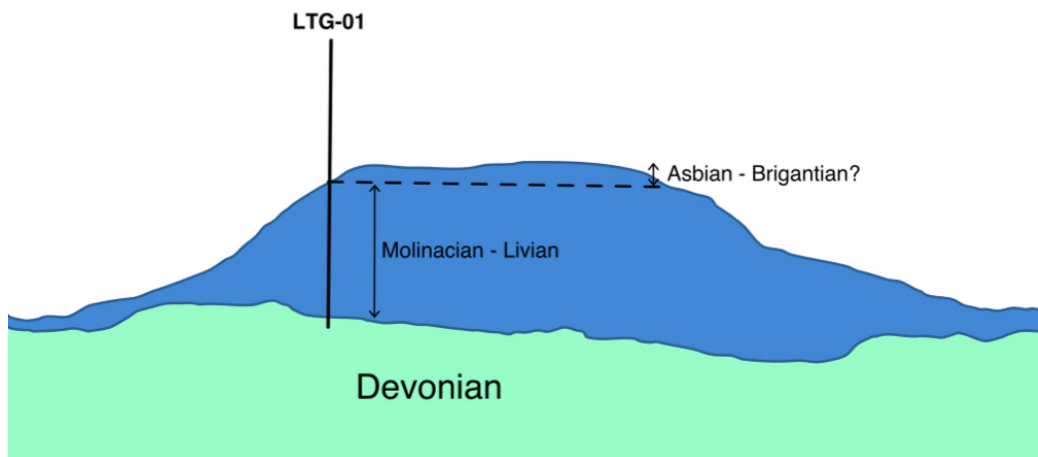


Figure 14: Simplified display of the location of well LTG-01 at the margin of the platform. Youngest sediments found in the well are Moliniacian to Livian in age, but Asbian - Brigantian sediments might be present in the top of the platform.

Stylolites are frequently observed in the core, both continuous through the rock as well as sutured contacts between grains. They occur often with authigenic euhedral quartz and are surrounded by organic matter (Mozafari et al. 2019). Vachard (2004) found traces of Tournaisian infill in tectonized limestone within the interval of 4440 to 4464 m, which could indicate karstification events. The paragenetic sequence constituted by Mozafari et al. (2019) consists of multiple phases of cementation and fracturing, and stylolitization. Early diagenesis in LTG-01 is characterized by an early marine cementation phase of fibrous and dogtooth calcite. Small vugs might indicate a minor phase of karstification, but were subsequently cemented by meteoric calcite cements (Mozafari et al. 2019). UHM-02 shows signs of dissolution enhanced fractures, but these are absent in LTG-01. During burial, the cementation of an equant calcite (C2) occurs, which replaces some aragonitic components and destroys the porosity in the rock.

A key observation in the core analysis is the presence of two phases of fractures:

1. Relatively rare complex fractures that are subvertical to subhorizontal, these pre-date the stylolites and are cemented by calcite and possibly dolomite.
2. Sub-vertical fractures which are cemented by calcite cement initially, and then locally by a later dolomitic cement. These post-date the stylolites and the other type of fractures.

The complex fractures that pre-date the stylolites have a possible karst origin (for example in UHM-02) as the cementation phase has been proven to be high temperature, $\pm 190\text{-}200^\circ\text{C}$, from hypersaline pore fluids (Goldberg et al. 2017). The post-stylolite, sub-vertical fractures were initially cemented by a calcite spar cement. They were reactivated and the cementation of two late saddle dolomites occurred (a ferroan dolomite and a non-ferroan dolomite; Mozafari et al. 2019). The condition of precipitation of these saddle dolomites is hard to derive. In UHM-02, morphology of the crystals suggests that they precipitated from pore fluids with a temperature higher than 60°C . This suggests that the dolomites are very unlikely to be early diagenetic in origin (Mozafari et al. 2019). It is therefore feasible that the dolomites are fracture fed, indicating possibilities for thermal fluids to flow through the host rock.

Pyrites were encountered in the samples. These could have formed in either an early stage of diagenesis (shortly after deposition) or in a later stage from thermochemical sulphate reduction at high temperatures. However, other features of thermochemical sulphate reduction such as anhydrite, galena, fluorite and others were not observed in the studied samples, and these pyrites were mostly found within clay fragments. This suggests that these pyrites originate from an early diagenetic stage (Mozafari et al. 2019). The minerals resulting from thermochemical sulphate reduction have been encountered in the nearby Derbyshire platform and are located in the matrix pores and fractures (Breislin et al. 2020). In case of LTG-01, it should be considered that mineral phases that crystallized from hydrothermal flows could have been missed in the drilled interval and that the pyrite content of this well is not representative for the whole area.

TNO performed clumped isotope analyses on fractures from samples from 4470.3 m depth in an unpublished study. Results suggest both the host rock and the first fracture cement phase occurred at high temperatures of 210 to 220°C . The clumped isotope temperature of these calcites is very close to the downhole temperature measurements that range from 186 to 203°C . The discrepancy between the measured downhole temperatures and the clumped isotope temperature could be due to the clumped isotope measurements having an error of $\pm 10^\circ\text{C}$ (which can be improved with more measurements) and downhole temperature having a standard deviation of ± 5 to 10°C (Bonté et al. 2012; Mozafari et al. 2019).

FMI logs were interpreted by Panterra. The results were published in a report by Van Leverink & Geel (2019). Over 900 fractures were identified in the well, with a fracture density of approximately 1.2 fractures per meter. Several clusters of fractures were identified. Van Hulten & Poty (2009) noted the correspondence with the gamma ray peaks of some of these fracture zones and interpreted them as karstification horizons. Oversteeg et al. (2014) suggested intervals showing signs of fracture permeability range within the depth interval of 4550 to 5150 m depth, implying a possible 600 m thick reservoir. Mud losses were encountered in the well; one at 4450 m (within cycle 3a), six between 4575 and 4700 m (2b, 2c, 2d), one at 4775 m (2b) and two between 4975 and 5025m (1c and

1d), which may indicate permeable zones. The base of the well shows high dolomite content, as was observed in the well log analysis by Mozafari et al. (2019). Dolomite has a higher fracture intensity than limestone under similar stress circumstances due to differences in rock strength, which can explain the higher fracture density at the base (Ortega et al. 2010). The positive thermal anomaly found by Bonté et al. (2012) could be explained by thermal convection, accommodated through fractures. Several fractures should be sufficient for this, provided that the fractures have good volumetric connectivity (Oversteeg et al. 2014; Lipsey et al. 2016). Van der Hoorn et al. (2012) performed a fault analysis study on LTG-01 to find whether the Dinantian limestones were suitable for reservoir stimulation and application of conventional hydraulic fracturing. It appears that this is the case and doing so can result in a feasible business case.

4.5 Global Dinantian platform models

Multiple different studies on other Dinantian carbonates have been done worldwide. Diagenetic studies were performed on the Viséan carbonates of the Derbyshire platform in the UK (Walkden & Williams 1991; Hollis 1998; Hollis & Walkden 2012), the Lower to Upper Carboniferous Precaspian Kashagan and Tengiz platforms in Kazakhstan (Ronchi et al. 2010; Collins et al. 2013) and the Viséan carbonate shelves and platforms in the Campine Basin in Belgium (Muechez et al. 1991a and b). Similar near-surface diagenetic features were described, such as early marine fibrous calcite, followed by meteoric dissolution and cementation that may be linked to karstification processes. In all platforms, early diagenetic phases are followed by later phases of cementation of calcite and saddle dolomite. Karstic dissolution that created significant early moldic porosity is well preserved in the Kashagan platform. Due to the similarities in age and encountered depth of the Kashagan carbonate platform, it provides a good analogue for this study. Dissolution vugs and channels (cm in size) developed locally below the sequence boundaries. Parts of the porosity was cemented by burial cements, but not blocked. Ronchi et al. (2010) found that reservoir quality was substantially poorer at the base and top of sedimentary sequence cycles of the platform interior, but the quality was high in between. This porosity cyclicity was created by the interaction of freshwater, resulting in either dissolution or cementation, along with compaction that destroyed parts of the porosity. In the margins of the platform, a more heterogeneous porosity distribution was found due to a stronger burial diagenetic overprint, which was linked to exotic fluid circulation. Basin-sourced fluids caused local dolomitization, dissolution and cementation here (which was also suggested for the Derbyshire platform by Hollis 1998). The margins of the Kashagan platform were preferential sites for the development of fractures and mineralization. These preferential sites have not been noted in the platforms of the Campine Basin and Derbyshire. The Campine Basin was more prone to burial diagenesis. Over time after meteoric cementation, pore waters in shelf carbonates became progressively more anaerobic, triggering neomorphism that resulted in non-, bright and dull luminescent cement stages. The dull luminescent stages represent a cement that formed in a meteoric fluid at $\pm 30^\circ\text{C}$ based on clumped isotope analyses, indicating burial diagenesis within the first 1 km. It is expected that gravity-driven groundwater flow from the London Brabant Massif played a very important role in the cementation of these shelf carbonates (Walkden & Williams 1991). The studied rocks showed a phase of fracturing that occurred before the precipitation of the meteoric cements, but it was not that intense yet. Substantial fracturing took place during the precipitation of the dull luminescent calcites, at the end of Viséan and Early Namurian times (Muechez et al. 1991a).

Fluid inclusions in the Derbyshire platform are characterised by temperatures from 57 to 200 °C with both low and high salinities (4.4-23% NaCl equivalent). The studies by Muechez et al. (1991a and b) found similar values for fluid inclusions, with temperatures of 50 to 150 °C for the calcites to 200 °C for the saddle dolomites. Fluid inclusions in the Kashagan platform were reported by Ronchi et al. (2010) and show high temperatures (70-120 °C) and low to moderate salinity (0-11% NaCl equivalent). Collins et al. (2013) studied fluid inclusions in the Tengiz platform and described much higher burial temperatures, reaching up to 226 °C.

5 Results and Interpretations

5.1 Petrographic analysis

Petrographic analysis was performed on thin sections and their photomicrographs to distinguish minerals and their diagenetic phases so that aimed quantitative petrography can be carried out on them. The paragenetic sequence is partially taken from Mozafari et al. (2019) and combined with the findings in this study. The result is shown and described in Table 2. Examples of different cement phases have been observed in photomicrographs, which are shown in Fig.15. These cements (C1a-b, C2 and C3) have destroyed the initial porosity of the rock matrix and the matrix therefore were not targeted with the quantification. Veins contain saddle dolomites that were cemented after reactivation (SD1, which is ferroan in nature and SD2 which is non-ferroan; Fig.16 & Fig.17). The veins were targeted in the quantification, as SD2 contains intracrystalline porosity. Part of this porosity was occluded by calcite cement (C4), which was not pervasive and some intracrystalline pores remain open.

1. Early marine cementation of fine, fibrous calcites (C1a)
2. Dissolution and meteoric dogtooth calcite cementation (C1b)
3. Cementation of equant calcite (C2), occluding primary porosity
4. Fracturing phase 1 (complex fractures) and calcite cementation in fractures (C3)
5. Chemical compaction; stylolites
6. Fracturing phase 2 and reactivation. Fracture cementation of saddle dolomites (SD1 & SD2)
7. Late intracrystalline porosity infill of calcite (C4)

Table 2: *Constituted paragenetic sequence with corresponding cement codes for Fig.15 in brackets*

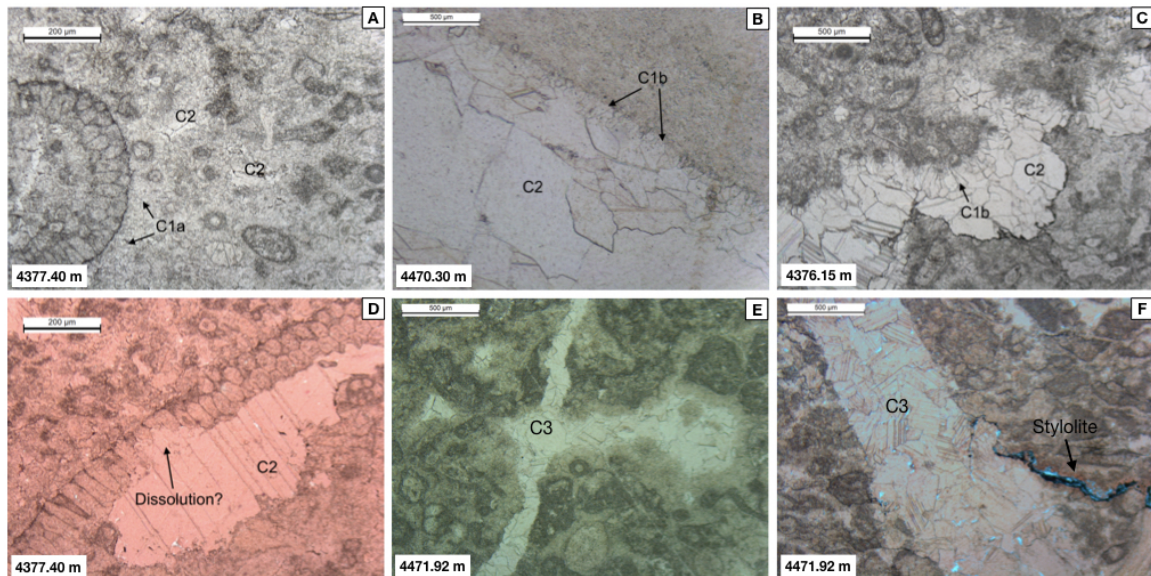


Figure 15: *Plane polarized light (PPL) images showing the types of calcite cements observed in LTG-01 thin sections. C1a is fine crystalline, fibrous calcite of marine early diagenetic origin. C1b is limpid dogtooth calcite of meteoric, early diagenetic origin. C2 is equant calcite that replaces aragonitic components and occludes primary porosity and was cemented during burial of the rock. C3 is calcite spar that cemented within the first phase of fractures. Note the fracture post-dating the stylolite in photograph F. Depths of the thin sections are shown in the corners of the photographs. Photomicrograph D is red due to staining.*

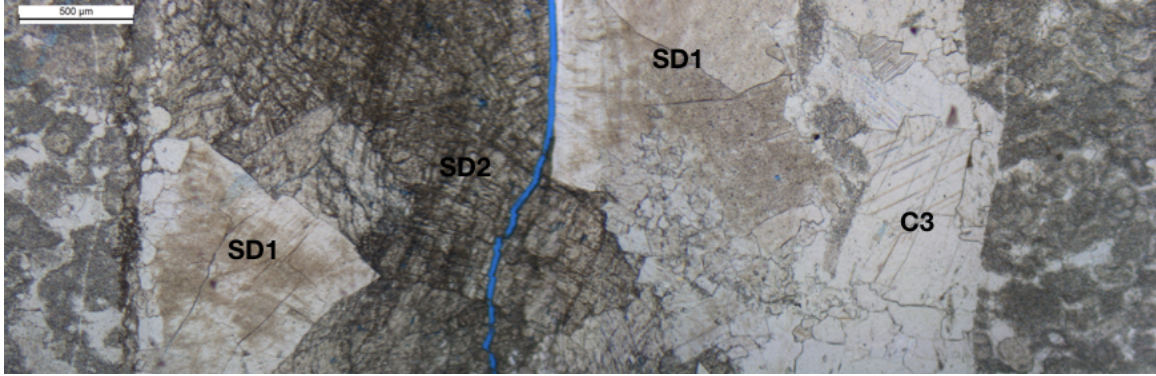


Figure 16: Photomicrograph of a vein in LTG-01 (depth 4470.30 m) showing multiple phases of cementation. Initial cementation of the vein C3 appears to be replaced by recrystallized SD1 and SD2. SD2 shows cleavage, which might indicate tectonic activity.

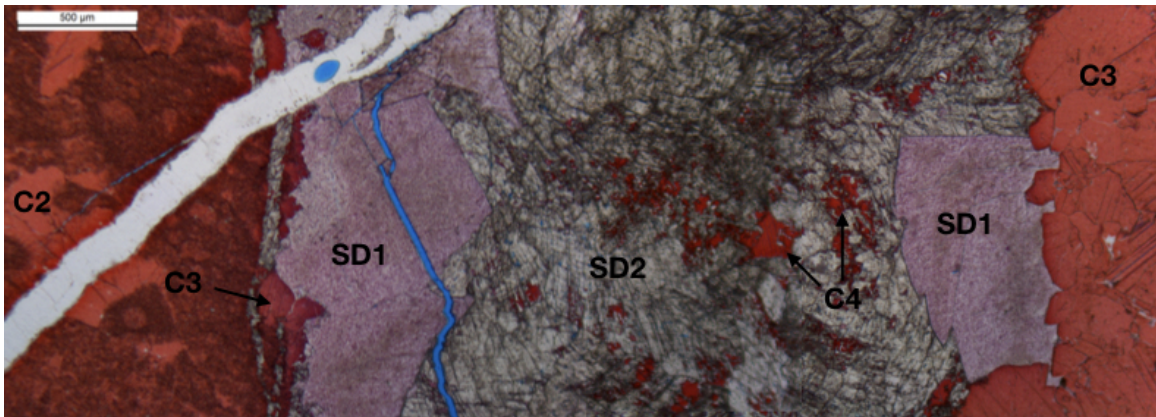


Figure 17: Stained photomicrograph of a vein in LTG-01 (depth 4470.30 m) showing the presence of later cementation phase C4 that occludes part of the intracrystalline porosity in SD2. Some intracrystalline porosity is preserved.

5.2 Quantitative petrography

The results of the quantitative petrography by point counting on the thin sections are shown in Table 3 to 6 (see Appendix B for point counting results on the photomicrographs). Table 3 shows the results of point counting done on thin sections which contain one or multiple veins, to estimate the volumetric part of veins in the host rock at that depth. No distinction of minerals or grains within veins or matrix was made. A relatively constant value with an average of 10% volumetric part of veins is observed.

Sample depth (m)	Vein	Matrix
4470.30	12%	88%
4470.63	15%	85%
4471.92	4%	96%
4472.02	10%	90%
4472.48	9%	91%

Table 3: Distribution of veins vs. matrix in thin sections containing one or multiple veins. On average, veins make up 10% of the volume of the rock at this depth.

For quantification of mineral content and porosity of the matrix, point counting was carried out (Table 4). This was done on photomicrographs of core 2 (4473 to 4470 m depth) as these rocks are located in a fractured interval. The point counting confirms the assumption that the matrix has no visible porosity. Cement phase percentages show overall comparable values.

Sample depth (m)	Porosity	Grains	C1/C2	C3
4470.30	0%	51%	21%	28%
4470.30	0%	48%	28%	24%
4470.63	0%	51%	30%	19%
4471.92	0%	45%	37%	19%
4472.02	0%	43%	37%	20%
4472.48	0%	51%	35%	14%

Table 4: Results of point counting on photomicrographs of thin sections ($n = 150$), focused on matrix of the rock. Veins were not included in the point counting. Matrix shows no visible porosity.

Photomicrographs representing (partial) vein infill have been selected for point counting (Table 5). Point counting on full thin sections was not possible since picture quality was too poor to distinguish multiple phases of cement within the veins. Phases C1 and C2 were observed at the edges of the vein and are assumed to predate vein reactivation. Largest infill of the veins is represented by SD1 and SD2, which were cemented after vein reactivation. Intracrystalline porosity was only observed within SD2, which shows cleavage. C4 occupies part of the intracrystalline porosity of SD2.

Sample depth (m)	$\phi(int.)$	C1/C2	SD1	SD2	C4
4470.30	5%	7%	29%	50%	9%
4470.30	7%	7%	21%	65%	0%
4470.63	3%	0%	7%	80%	10%
4470.63	5%	0%	0%	76%	17%

Table 5: Results of point counting on photomicrographs of thin sections ($n = 150$), focused on infill of veins. Rock matrix is not included in the point counting. Cements are in chronological cementation order (C1 is earliest, C4 is latest).

Cuttings are no favorable source of data in terms of finding fractures or veins as these structures are not preserved. However, content of mineral phases still provides necessary information as no core slabs could be retrieved from the depths other than the intervals of core 1 and core 2. Therefore, point counting on cuttings was carried out on intervals of interest, based on fracture intensity and higher dolomitic content according to Mozafari et al. (2019) (Table 6; Fig.18). It should be taken into account that the depth of the cuttings is not absolute, but rather indicative. Slight deviations should thus be taken into account. Cuttings from the fractured interval (4450 to 4800 m depth) do not provide much information on the fractures and/or veins, as these structures are not preserved. The cuttings at 4520 m and 4570 m show no major dolomite content. An increase in dolomite content can be observed in a cutting from 4650 m depth. In the interval from 4990 to 5100 m dolomite content increases, with values up to 40% at 5066 m depth.

Intracrystalline porosity could not be observed in thin sections from the interval, since no core could be retrieved. Some porosity in small fractures is observed in the cuttings, but this is likely (and therefore assumed) to be a result of preparation of the material.

Sample depth (m)	Calcite	Dolomite	Quartz	Opq
4520	95%	5%	-	20%
4570	59%	9%	12%	8%
4600	83%	9%	-	-
4650	84%	16%	-	-
4768	92%	8%	-	-
4800	86%	14%	-	-
5010	79%	21%	-	-
5052	93%	7%	-	-
5066	39%	27%	31%	3%
5076	85%	15%	-	-
5082	85%	13%	1%	-

Table 6: *Results of point counting on cuttings. Upper part of the table shows cuttings from the fractured interval (4450 - 4800 m), and bottom part of the table is represented by the dolomitized interval (5000 - 5100 m). Opq stands for opaque minerals. A distinction between opaque minerals is deemed unimportant for this study.*

5.3 Well log and FMI integration

Fracture density in the well was measured per meter (Fig.18). The synthesis of previous work showed that a positive relation between fracture density and dolomitized limestones exists. Petrophysical analysis suggests porous zones around 4470 m (2d-3a cycle boundary), 4580 m (2c-2d cycle boundary), 4770 m (just over 2a-2b cycle boundary) and 4490 m (1c-1d cycle boundary). These zones appear to match the zones of increased dolomitization (Fig.19). The cuttings from the shallower interval show no interesting dolomite content, which is in line with the fracture density at this depth interval. At 4470 m, fracture porosity shows minor peaks in the FMI. The sequence boundary between cycle 2d and 3a is also located here. The platform depositional setting did not change between these cycles, but cycle 3a is the only cycle that showed indications of karstification. Quantitative petrography showed 10% vein volume at this depth is also in line with the FMI, where a fracture density of 1 to 2 fractures per meter can be observed (Fig.18). At 4580-4600 m, two minor mud losses are recorded (3.000 L and 2.000 L). This is located at the sequence boundary between cycles 2b and 2c, where the depositional setting changed from a high energy setting to a low/moderate energy setting. Just above and below this depth, intervals with peaks in fracture density can be observed (Fig.18) and fracture porosity shows high values just above the sequence boundary. This coincides with the sequence boundary between cycles 2c and 2d, where the platform changed from a low/moderate energy setting to a high energy setting. At 4650 m depth, the FMI shows a high fracture density (up to 7 fractures per meter). A major mud loss (30.000 L) was recorded here and the cuttings data show a relative increase in dolomite towards 16% at this depth. From 4760 to 4800 m, fracture density is either 0 or has not been recorded. However, fracture porosity shows the highest measured values here. A mud loss of ± 41.000 L is recorded at this depth; this is the largest mud loss in the Dinantian interval of LTG-01. It is thus likely that fracture density was too high to record. This fractured interval is observed just at the boundary between cycle 2a and 2b, where the depositional environment transitioned from inner ramp to a more marginal setting.

Summarizing, in the interval from the top Dinantian to 4800 m fracture porosity is largest in the intervals 4470 - 4500 m, 4570 - 4600 m, 4760 - 4800 m with some (but low) fracture porosity in between the intervals. All these zones coincide with sequence boundaries where the depositional setting of the platform changed. Another noteworthy observation is made at a depth of 4680 m within cycle 2b, with a peak in fracture porosity, fracture density and a record of a mud loss (2000 L). No cuttings were retrieved from this depth.

The base of the Dinantian limestone (4990 to 5123 m) shows an interval with very clean and low GR. Fracture porosity and fracture density show a large increase. Major part of the fractures are partially conductive and multiple fracture clusters are observed in the FMI. These are found at 4990 m, which is the boundary between cycle 1c and 1d, and the interval of 5075 to 5120 m. A minor

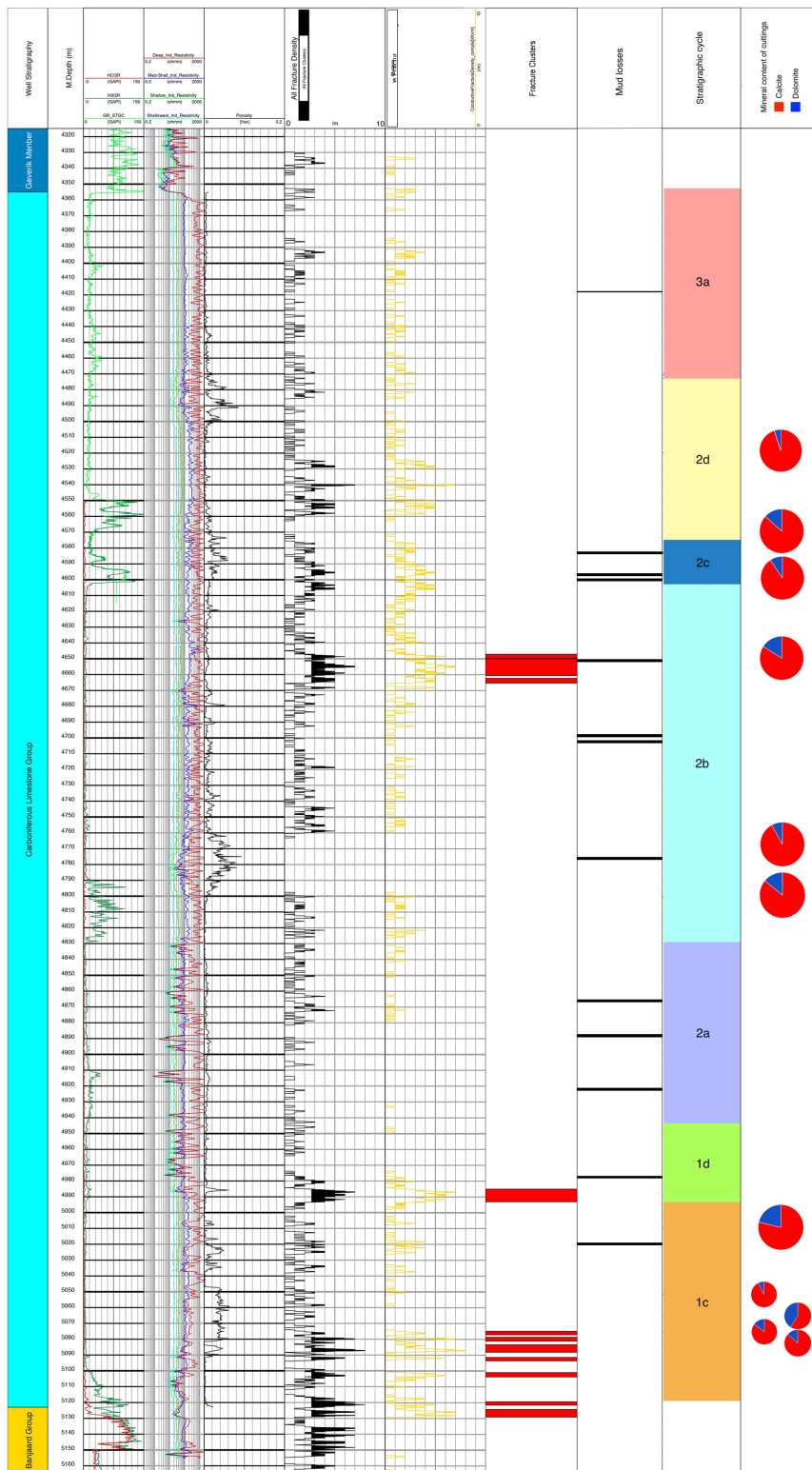


Figure 18: FMI log of LTG-01. Columns from left to right: Well stratigraphy; depth (m); Gamma ray; Resistivity; Fracture porosity (all fractures); Fracture porosity (conductive fractures; Fracture clusters; Mud losses; Stratigraphic cycle; Calcite/dolomite ratio derived from quantitative petrography on the cuttings. Modified after Van Leverink & Geel 2019.

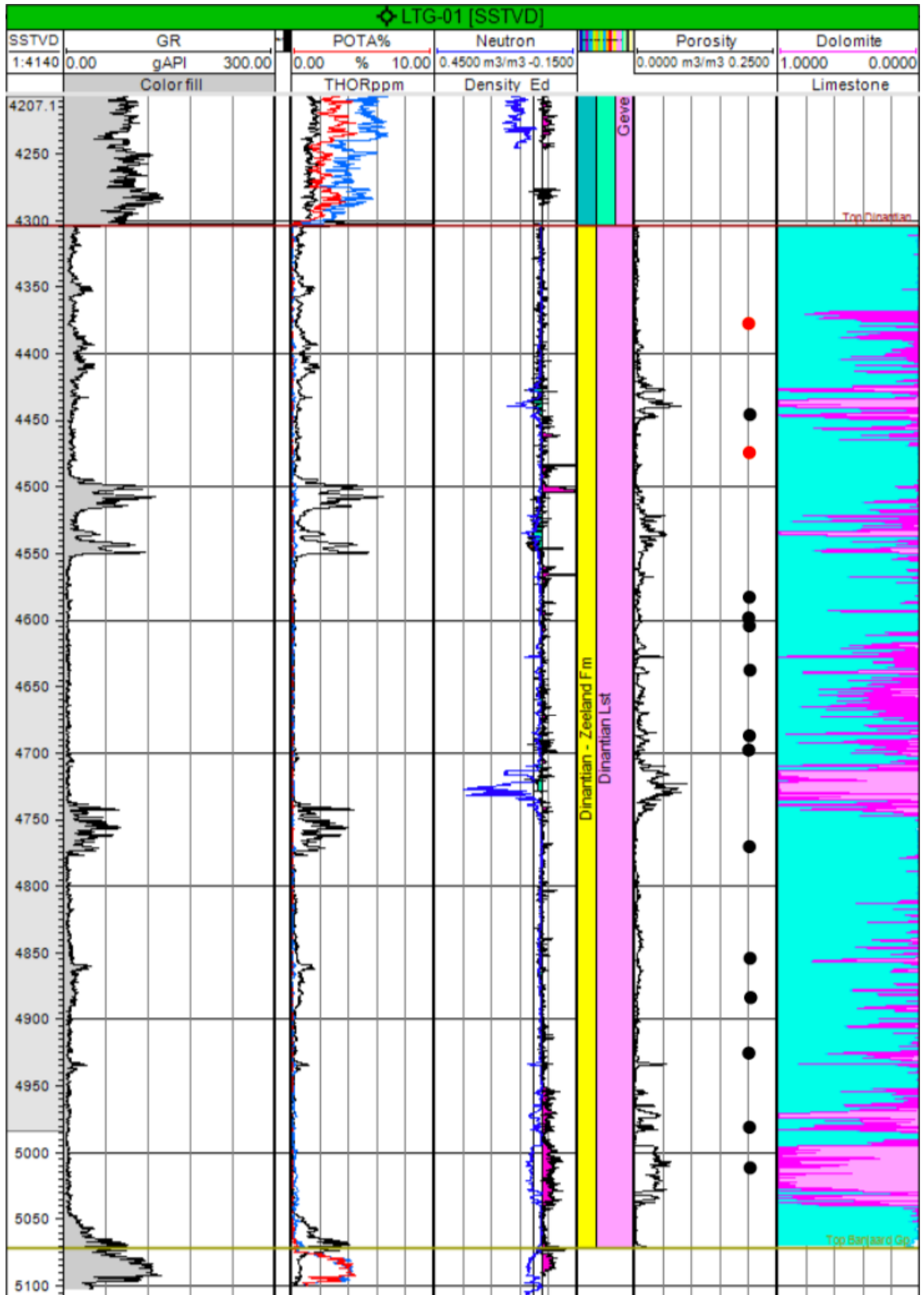


Figure 19: Gamma ray, neutron/density, porosity and mineralogical logs in the LTG-01 well. Dolomite proportions are shown in the right column in pink. Locations of mud losses are shown by black dots in the porosity column. Red dots indicate the locations of the slabbed cores. Modified after Mozafari et al. 2019.

mud loss of 600 L is recorded at 4990 m, faults recorded at this depth are (partially) conductive. Another mud loss (1000 L) was recorded at 5020 m, no cuttings were retrieved from this depth. Fracture porosity shows even greater spikes around 5060 m. A cutting at 5066 m shows dolomite content of 40%. The FMI shows appearance of vuggy zones from 5010 to 5090 m which match with zones of increased fracture porosity.

5.4 Seismic interpretations

5.4.1 Faults and seismic horizons

Interpreted horizons of the top and base of the Dinantian interval are in line with horizons proposed in earlier studies and clearly show the top and base of the isolated platform (Fig.20). In the margins of the platform multiple large scale faults have been interpreted based on distortions in reflectors (Fig.21). The faults continue into the overlying, younger strata. From the seismic profiles, the faults appear to be rooted in the older Banjaard group. A clear offset of the base and top of the platform could not be observed. The seismic profiles are 2D, so the exact orientation and strike of the faults could not be derived. However, the faults appear to have a \pm NW-SE strike, which is in line with the inherited structure of subsurface during the formation of the NWE CB (De Jager 2007; Kombrink 2008; Van Hulten 2012). These faults were originally extensional, but some show a reverse offset, which can be linked to the later inversion of the area in the Oligocene (De Jager 2007).

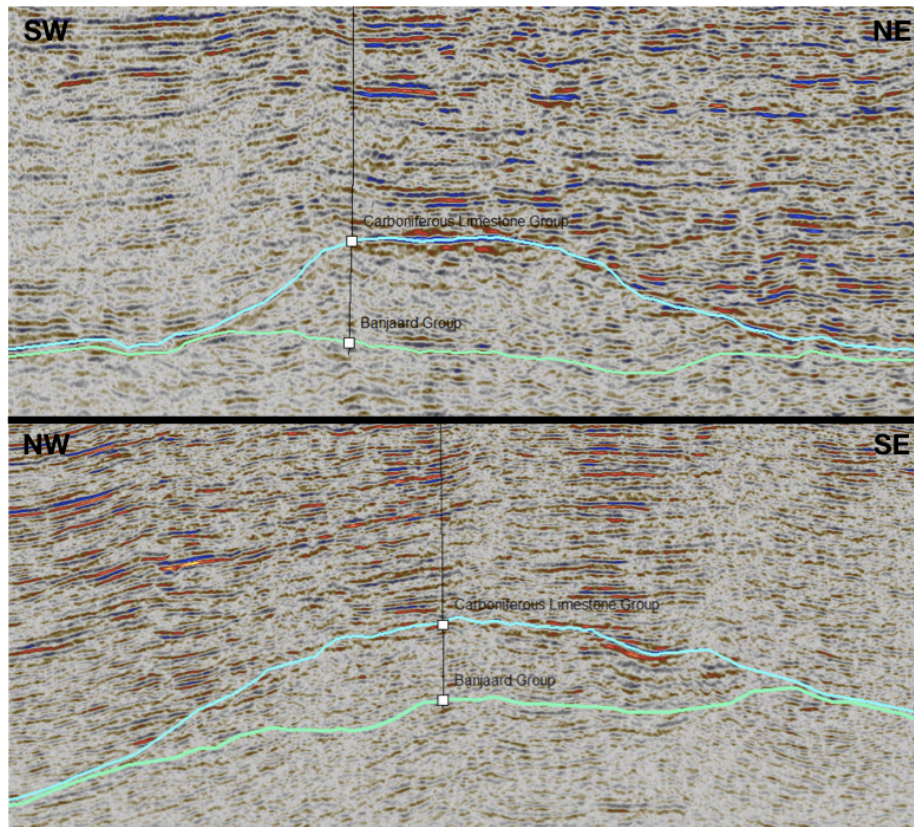


Figure 20: SW to NE and NW to SE seismic lines through Luttelgeest platform. Black vertical line indicates the position of well LTG-01. Light blue horizon indicates the interpreted top Dinantian, the green horizon indicates the interpreted base of the Dinantian.

On a smaller scale, multiple faults were observed and interpreted in the margin of the platform (Fig.22). All faults have similar geometry and appear to dip northward, it is not clear whether the faults cross the top or base of the Dinantian.

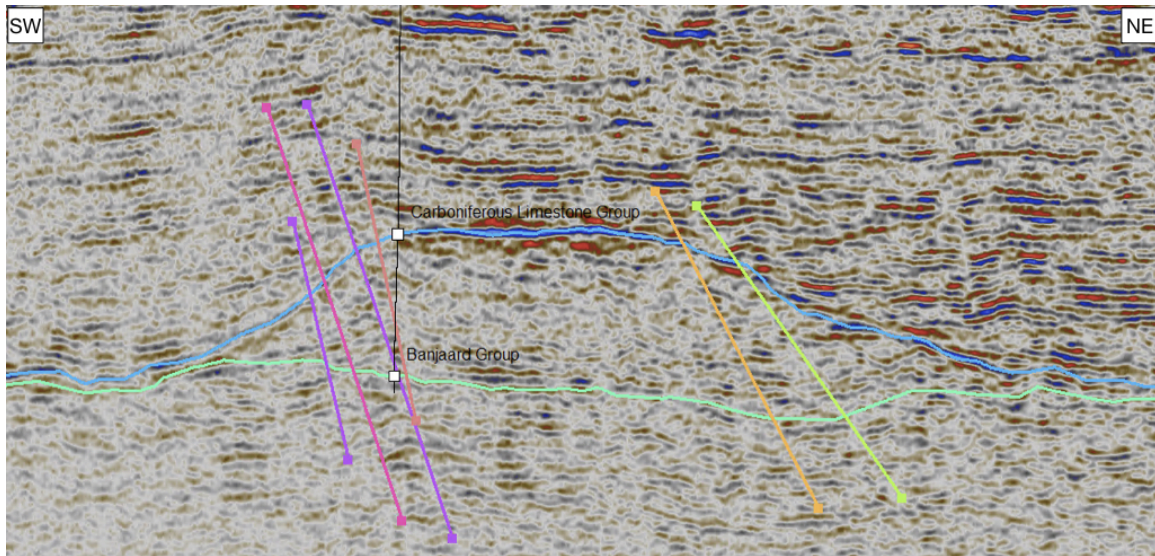


Figure 21: *Interpreted faults in the northern and southern margins of the platform. Faults appear to root into the older Banjaard group, below the Dinantian limestones.*

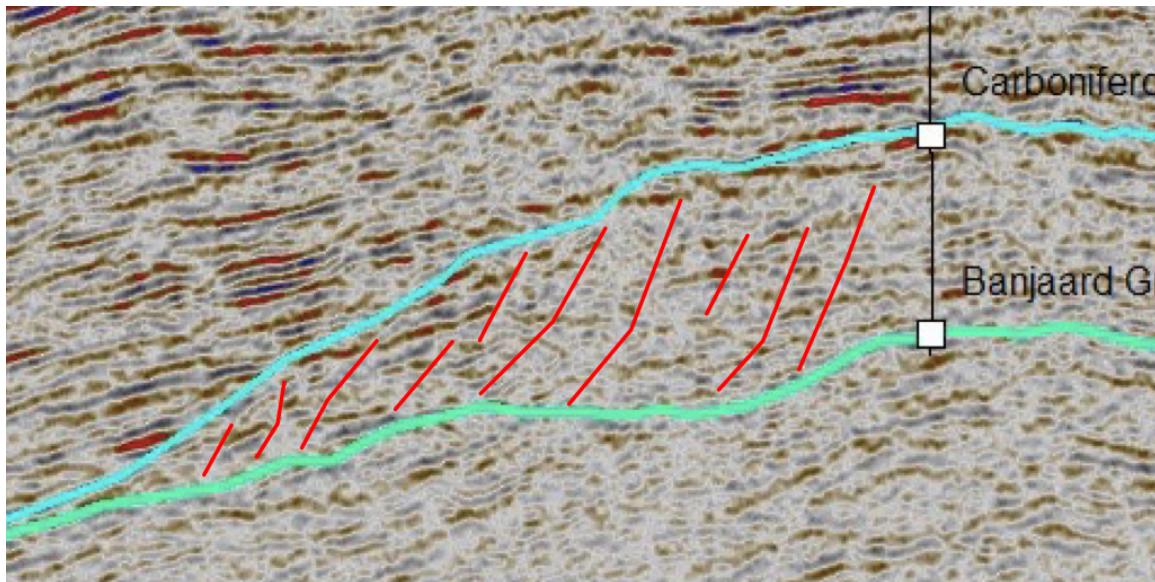


Figure 22: *Interpreted smaller scale fractures (red lines) in the margin of the Luttelgeest platform. Blue line indicates the top Dinantian, green line indicates the base Dinantian.*

Continuous reflectors within the platform structure are difficult to track since their acoustic impedance (AI) is very low and they have a relatively chaotic character, but with detailed analysis some horizons could be traced and interpreted (Fig.23 & Fig.24). Note that the orientation of the faults can be linked to the aforementioned extension, creating normal faults with a NW-SE strike. The interpreted horizons coincide with sequence boundaries constituted by Mozafari et al. (2019). The top horizon is easily traceable in the SW-NE section, but more difficult in the NW-SE section. At the intersection of the well the horizon could be placed due to the known location of the sequence boundary, but it is hard to track from there and therefore uncertain.

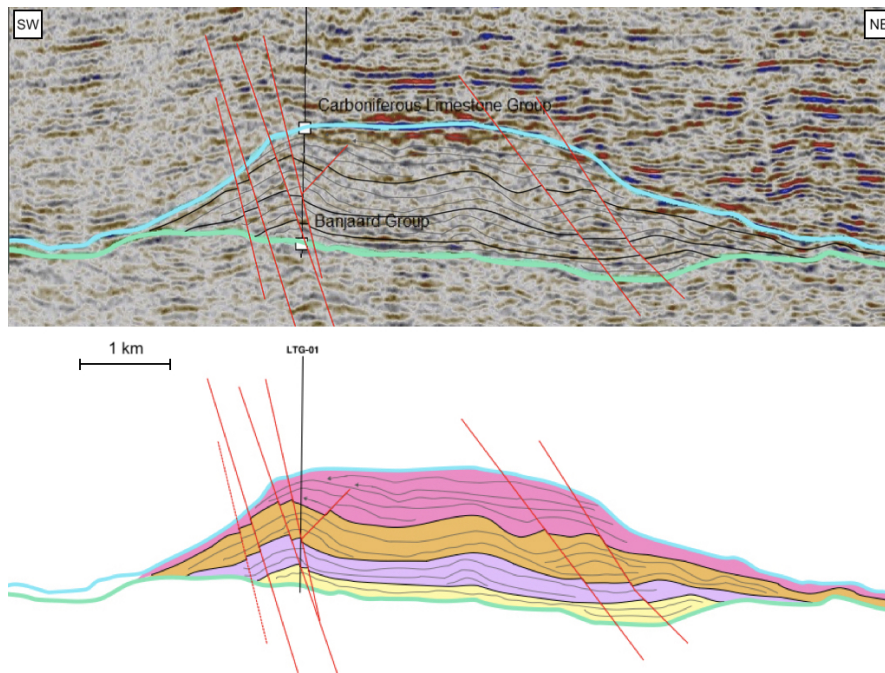


Figure 23: Interpretation of horizons of SW-NE seismic section through the Luttelgeest platform. Yellow area indicates cycles 1c and 1d; Purple area indicates cycle 2a; Orange area indicates cycle 2b; Pink area indicates cycles 2c, 2d and 3a. Arrows indicate onlap onto older deposited sediments, red line indicate interpreted faults.

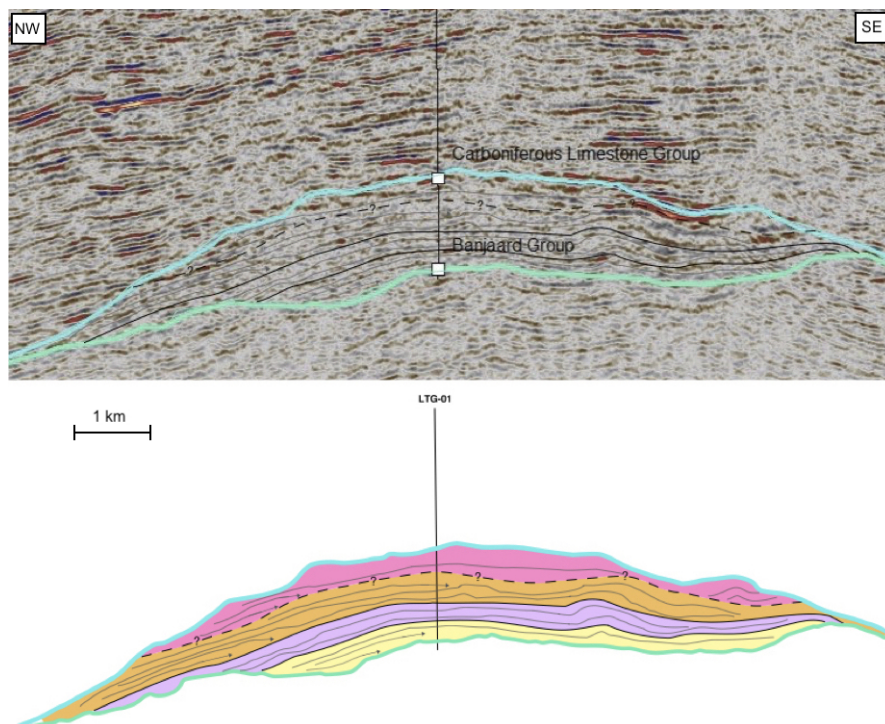


Figure 24: Interpretation of horizons of NW-SE seismic section through the Luttelgeest platform. Yellow area indicates cycles 1c and 1d; Purple area indicates cycle 2a; Orange area indicates cycle 2b; Pink area indicates cycles 2c, 2d and 3a. Top horizon was harder to differentiate and has therefore been annotated with a dashed line. Arrows indicate onlap onto older deposited sediments.

One of the faults crosses the well at ± 4800 m depth. An interval with high GR is observed here (Fig.25). This is also the location of the boundary between sequence cycles 2a and 2b which has been interpreted by Mozafari et al. (2019) to be a transition from carbonate ramp environment to a carbonate shelf environment. The largest mud loss in the well (± 41.000 L) was recorded here.

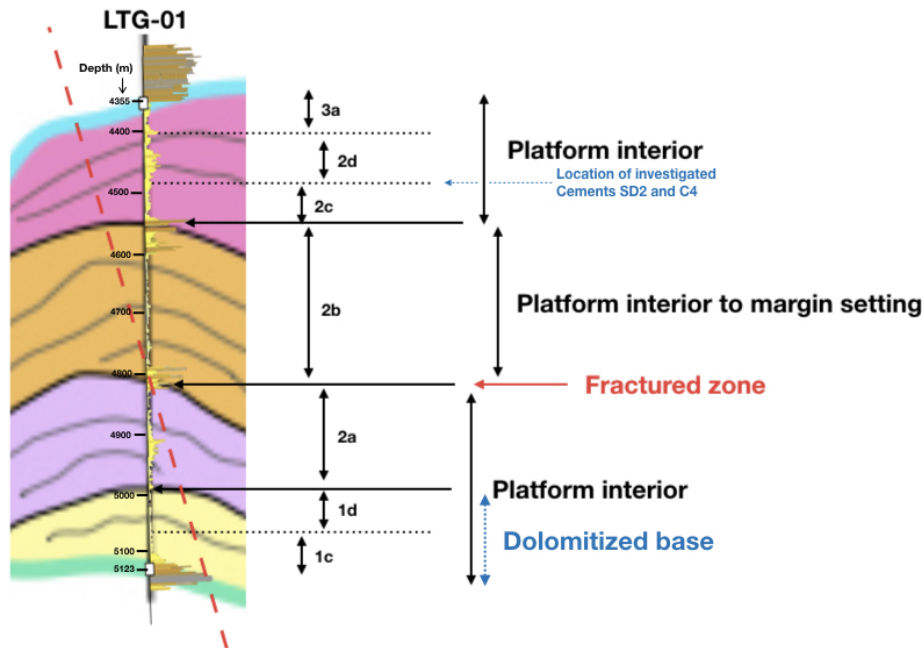


Figure 25: Zoomed in part of the platform. Figure shows one interpreted fault crossing the well, interpreted horizons and the GR projected on the well. The fault (red dashed line) crosses the well at the 2a-2b cycle boundary, where the depositional setting changes. From the FMI, the location where the red fault crosses the well, Fig.18 shows high fracture porosity at this depth. Also note the increase in GR. The largest mud loss is also recorded at this depth.

5.4.2 Seismic facies associations

Within the platform, multiple different seismic facies can be distinguished, based on reflector configurations and properties. These are shown and described in Fig.26. The seismic profiles were analysed and seismic facies were attributed locally (Fig.27) to characterize them and create facies associations with integration of the known data.

A clear distinction can be made with SF1 and SF2, which indicate the platform top and margins respectively, at the time of drowning of the platform. The strong AI indicates a large density difference which shows the transition from the soft Namurian shales to the hard Dinantian limestones. This is strengthened by the large change in GR value in the well log and the surrounding reflectors overlapping on the reflectors.

SF3 shows continuous, straight reflectors with a moderate AI and a moderate frequency which are interpreted as a platform interior. Looking at the NW-SE profile, SF3 is mostly found on the continental high and not basinward. SF3 is mostly found in the center and well correlation indicates a high energy platform interior setting. The development of clear, parallel reflectors indicates a good establishment of the interior setting.

SF4 is difficult to interpret due to its very chaotic nature and a very low continuity and AI. Well integration cannot be done properly because it does not cross an area with the SF4 association. However, interiors of carbonate buildups can show very low amplitude divergent reflectors (Macurda et al. 1997). According to Mozafari et al. (2019), this can occur due to patchy development (in contrary to the better development of SF3) of the carbonates or karstification related to high order depositional cycles. SF4 is not observed near the platform margins and appears to fill up space in the interior of the buildup and is interpreted as a platform interior facies.

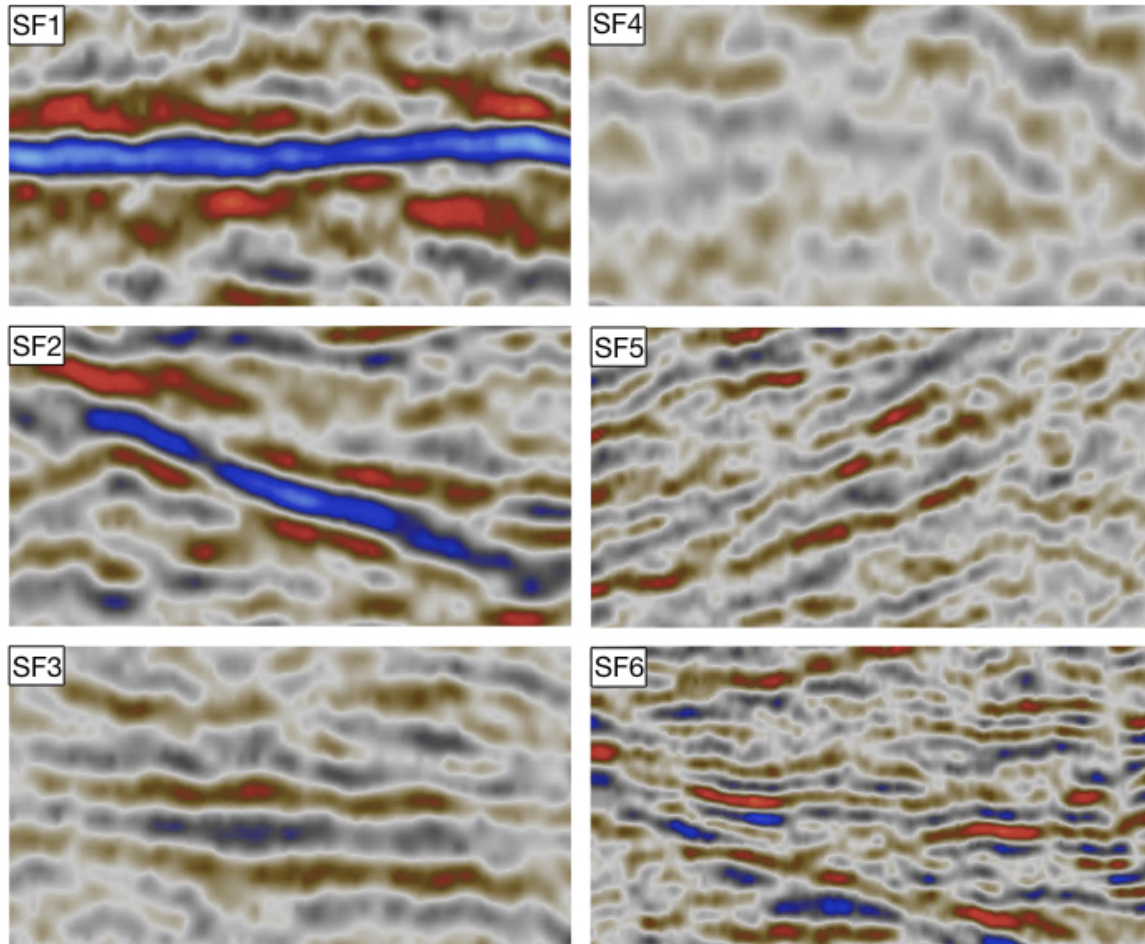


Figure 26: *Differentiation of seismic facies (SF) observed within the Luttelgeest platform based on reflection configurations: (SF1) Continuous, straight reflectors with high AI and a low frequency. Very outstanding reflector in comparison to others; (SF2) Continuous, inclined reflectors with high AI and moderate frequency. Surrounding reflectors appear to onlap and downlap on this facies; (SF3) Continuous, straight reflectors with a moderate AI and a moderate frequency; (SF4) Discontinuous, very chaotic reflectors with a low AI and low frequency. Many reflectors are divergent and terminate onto other reflectors within the seismic facies; (SF5) Relatively continuous, inclined reflectors with high AI and high frequency. Reflectors appear to terminate on reflectors within the seismic facies as well as surrounding seismic facies; (SF6) Continuous, straight reflectors with relatively high AI and a high frequency. The reflectors terminate onto the reflectors of SF2.*

SF5 shows relatively continuous, inclined reflectors with moderate to high AI and a moderate frequency. The facies hosts onlapping reflectors. In the first cycle of deposition (yellow area in Fig.24) the reflectors show that deposition onlapped to the structural high from the NW. This onlap is typical for SF5 and shows the expansion of the platform and onlapping deposition of carbonates on the created highs and is interpreted to represent the margin of the platform at a certain time.

SF6 represents the onlapping Namurian shales onto the Dinantian platform after drowning.

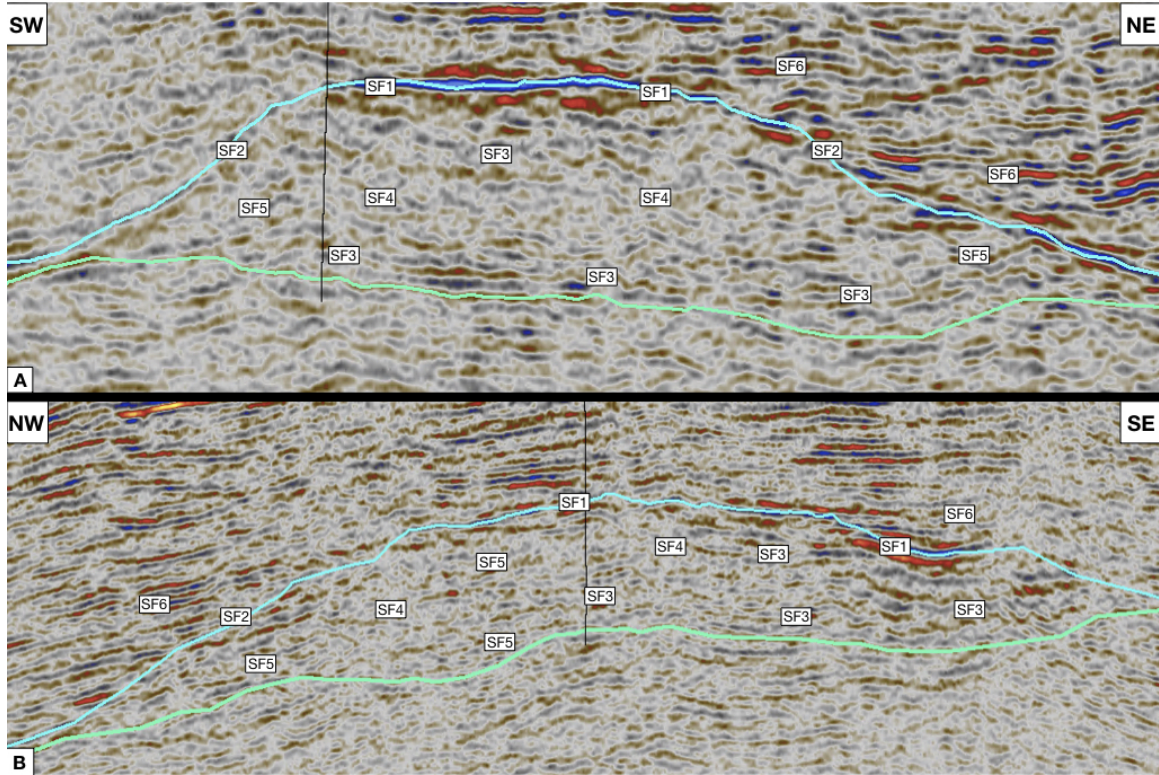


Figure 27: (A) Attributed seismic facies to the SW-NE seismic profile; (B) Attributed seismic facies to the NW-SE seismic profile.

6 Discussion

6.1 Dolomitization and impact on reservoir properties

Dolomites have been reported and investigated in LTG-01 borehole, principally as fracture/vein-related cement filling (SD2, see above) and massive rock-interval - the latter being present at the base of the borehole. The intracrystalline porosity in SD2 is the only porosity observed in the rocks (apart from measured fracture porosity in the FMIs). The relation between the dolomite SD2 and calcite cement C4 is something that needs more focus, as these porous zone could be a possible target for geothermal application. C4 does not occlude all intracrystalline porosity observed in SD2 (Fig.28), but was certainly cemented in a later stage since it fills the intracrystalline pores of the former as it has been demonstrated in the Results section. Original intracrystalline porosity of SD2 is therefore assumed to have been substantially higher, with values ranging from 9% up to 17% of intracrystalline porosity in the initial vein, based on the quantitative petrography carried out. Also, SD2 shows signs of corrosion, which could bring up the question whether parts of SD2 were dissolved in a certain phase, which was then followed by the cementation of C4 in (parts of) the created intracrystalline porosity. Further geochemical (e.g. stable C and O isotopes) and fluid inclusion analysis (e.g. microthermometry and crush-leach) would help place the timing of the dolomitization. In addition, understanding the origin of C4 and its distribution may help in mapping or finding similar veins filled with SD2 that have not been subjected to the cementation of C4. Such areas can be important pathways for fluid flow and thus are interesting targets for geothermal energy application.

Summarizing, the Dinantian interval hosts two dolomite phases. Firstly, there is the reported vein-filling dolomite phase, showing significant intra-crystalline porosity which was constrained over time by the later calcite cement C4. If areas with similar dolomite phases without the C4 infill exist throughout the reservoir, they can be attractive targets for fluid flow. Secondly, there is the massive

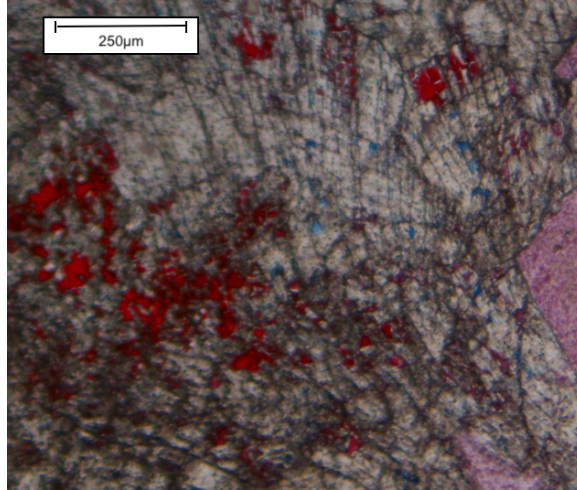


Figure 28: *Zoomed in photomicrograph of a vein at 4470.30 m depth, showing C₄ (red cement) not occluding all intracrystalline porosity (blue) in the SD2 (white/grey cement). Original intracrystalline porosity of SD2 is assumed to have been substantially higher before cementation of C₄.*

dolomite rock interval at the base of the well. Previous work investigated the interval and the quantitative petrography on cuttings of this study confirmed the high dolomite content in the base 120 m of the well. High fracture porosity values argue for a possible use of geothermal application in this zone.

The question now rises whether a link can be established between the saddle dolomites observed in the veins and the dolomites at the base of the well. If these dolomites at the base (of both UHM-02 and LTG-01) are genetically related to the saddle dolomites in the fractures, it is probable that dolomitization at the base post-dated the C3 calcite cementation phases within the veins, which would be an indicator for the syn-tectonic nature of the dolomites. An intracrystalline porosity network could then exist in the base, but it is uncertain whether these have been affected by cementation of C4 like observed in the core samples. Future investigations on the origin and distribution of C4 could help predicting where porous zones exist so they could be considered for geothermal development. The FMI shows increased porosity values in the base of the well, which could be linked to such secondary (intracrystalline) porosity. Ortega et al. (2010) showed a positive relation between fracture intensity and dolomitized Lower Carboniferous carbonates in southern Belgium, which might explain the increase in dolomite content accompanying the high fracture density and porosity in this interval.

6.2 Implications of fractures as potential flow pathways

The studies on the Kashagan and Tengiz carbonate platforms (Ronchi et al. 2010; Collins et al. 2014) showed that the best reservoir quality was observed in the platform margins as these were preferential sites for faults to develop. The reservoir quality of Tengiz is positively affected by the progradational sequence (Harris 2008). These slope sediments are deposited in a relatively high energetic environment, which gives coarser grains with more initial porosity. Apart from that, slopes become unstable and collapse, creating faults (that can also be reactivated later) and thus possible increase in porosity and permeability (Reijmer et al. 2017). This is also the case for the Tengiz platform, where multiple open fractures are observed in the platform margin (Fig.29). Similar types of faults were observed in the NW-SE seismic profile of the Luttelgeest platform (Fig.22). These faults are, like the Tengiz platform, located in a progradational sequence in the margin of the platform. As mentioned before in Section 2.1, tectonics quiescence and further burial of the Dinantian occurred from about 326 to 313 Ma, during which a probable sealing of fractures

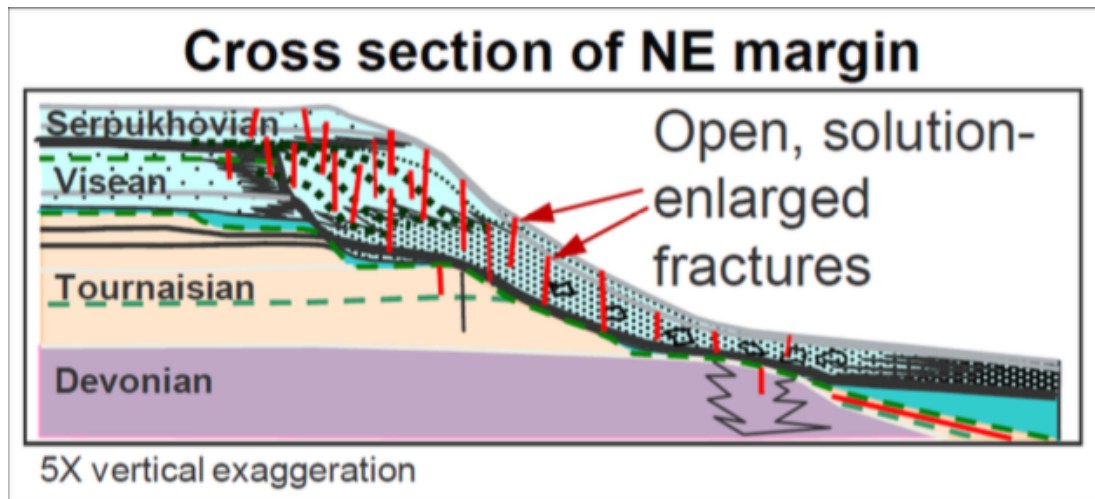


Figure 29: Locations of open fractures in the margin of the Tengiz carbonate platform. The fault geometry shows similarities to the faults observed in the margins of the Luttelgeest platform (Fig.22). From Harris (2008).

by cementation occurred (which would relate to the cementation of cement C3; Kombrink 2008, Mozafari et al. 2019). Later on with the upcoming tectonic deformation associated with the Permian uplift and wrench faulting (Geluk 2007), the investigated Dinantian platform was further deformed, and the existing cemented faults and veins might have been reactivated since that time, resulting in a relative increase in fracture porosity. The faulted margin of the Luttelgeest platform should therefore remain an area of interest and subject to subsequent studies on the Luttelgeest platform as it shows possibilities for the appliance of geothermal energy. It should be noted that beside being possible fluid pathways, faults can also pose a threat for sealing capacity (Harris 2008).

This study is mainly focused on fractures in the southern margin of the platform due to the possibility to integrate well data. Other studies also already mentioned a fractured southern margin (Hoornveld 2013; Mozafari et al. 2019). However, fractures in the northern margins were also interpreted in this study (Fig.21), but could not be integrated with well data due to great lateral differences. A study on seismic reprocessing of the same area done by Carpentier & Steeghs (2016) also clearly shows the large scale discontinuities in the seismic reflectors, which are interpreted as large faults crossing the Dinantian interval (Fig.30). The observation of the faults continuing into the older sediments below might be important as these could be or could have been hydrothermal fluid pathways altering the Dinantian limestones. The full composite log of LTG-01 shows presence of pyrite in the underlying Banjaard sediments. Further research could investigate the origin of these pyrites. If these pyrites are of hydrothermal origin and are genetically related to the pyrites encountered in the Dinantian interval, it could indicate that hydrothermal flow from Devonian sediments through large fractures could have occurred. In the Derbyshire platform Hollis & Walkden (1996) found shows of fluorite and galena in fractures that were precipitated by hydrothermal fluid flows, which were linked to an underlying igneous body. Sissingh (2004) argued for presence of volcanic activity in well NAG-01 (which is close to LTG-01), so further research in mineral content of LTG-01 could point out whether such activity could have resulted in fluid convection through faults in the platform.

Another key indicative observation for the presence of earlier fluid flow has been the ferroan nature of dolomite cement SD1, implying the presence of iron-rich fluids which could come from clastic sediments. If the cementation of SD1 can be linked to the movement of fluids from the underlying Devonian clastic sediments, a timing of fracturing and hydrothermal flow could be established. However, Devonian paleogeography of the Netherlands is still uncertain. Geluk et al. (2007) argued for the presence of Devonian carbonate buildups below the Uithuizermeeden platform, while the sediments below the Luttelgeest platform were of a more clastic nature (Fig.31). This is based on wells in Belgium and the UK hence a lot of uncertainties exist in that interpretation. Well LTG-01

only touched the tip of the Devonian Banjaard group and showed clastic content, but the real nature of these sediments still needs to be defined. Studies on this could give more insight in Devonian paleogeography and its influence in affecting possible overlying Dinantian reservoirs through larger faults. Accurate mapping of the faults (e.g. through 3D seismic surveys) will help providing an optimal flow model for geothermal applications.

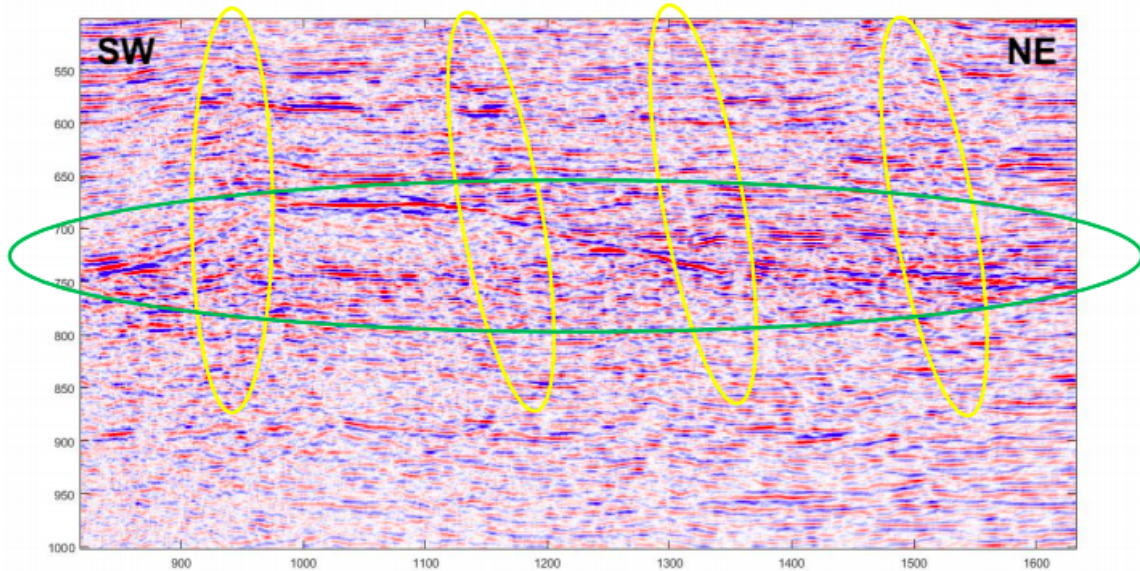


Figure 30: Reprocessed seismic image of the Luttelgeest platform. Indicated areas show zones of reflector discontinuities that can be interpreted as large scale faults. Note the location of the fractures in the northern and southern margins of the platform. Also note that the faults appear to continue into the younger Namurian and the older Devonian sediments. From Carpentier & Steeghs (2016).

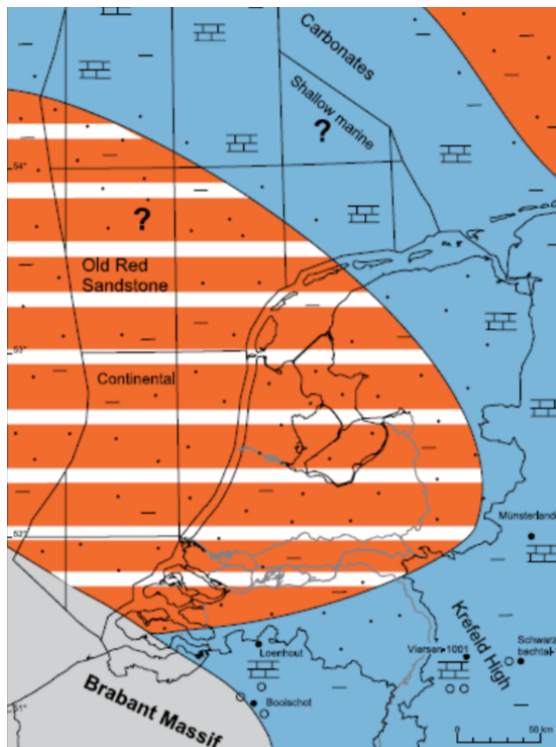


Figure 31: Paleogeographic map of the late Middle to early Late Devonian. The brown/white area shows the expected extent of the continental, siliciclastic Old Red Sandstone. Blue area shows the presumed occurrence of Middle Devonian carbonates. The interpretation is based on limited amount of wells, hence the question marks in the figure (Geluk et al. 2007).

6.3 Implications of stratigraphic boundaries as potential flow pathways

By extensive study of Mozafari et al. (2019) on the depositional environment of the carbonates of LTG-01, they showed that the major part of the well represents a high energy platform interior. The matrix of the rock appears to be fully cemented. Sarg (1988) argued that high energetic environments result in more water circulation, causing higher cementation rates. Lower energetic environments can remain uncemented for a longer period of time. It could therefore be argued that more quiet parts of the platform could have undergone less early cementation and therefore have a higher initial porosity. This could explain the relative porosity increase within cycle 2c, which has a low energetic depositional environment. The adjacent cycles, 2b and 2d, were deposited in a higher energy setting.

A trend between the relative increased fracture porosity and density at the location of sequence boundaries is suggested based on the FMI logs (Fig.18). It can be observed at the sequence boundaries 1c-1d, 2a-2b, 2b-2c, 2c-2d and 2d-3a. Changes in depositional setting can be small, but enough to create a heterogenetic boundary, which are interpreted as the sequence boundaries. These heterogeneities are relatively weak zones and fractures are thus more likely to develop there, which could explain the increase in fracture porosity in these zones. When looking at the dolomite content in Fig.19, there is also a clear trend in increase of dolomite content and fracture porosity (of which the peaks are located at the sequence boundaries). If the boundaries are indeed fractured, these fractured zones could have been pathways for fluids, resulting in the higher dolomite content we observe. It should therefore be taken into account that not only large fault systems, but also stratigraphic boundaries could play a large role in the fluid flow in a reservoir.

As observed in the SW-NE seismic profile, a fault crosses the well at the depth interval of 4780-4800 m. This is also the depth interval of the sequence boundary between cycle 2a and 2b, where the platform setting goes from an interior to a slightly more marginal setting (Fig.25). The high fracture porosity values and the largest mud loss indicate the possibilities for fluid flow to occur. The question rises how fluids, if injected through LTG-01, will flow. This study argues for the possibility to have fluid flow occur through sequence boundaries. It could however also be possible that fluid flow will occur along the fault plane.

6.4 Proposed conceptual model for potential fluid flow pathways through Dinantian carbonate reservoirs

Based on the previously discussed questions and the quantitative analyses achieved in this project, a conceptual model for flow pathways in the Dinantian is proposed, showing two scenarios (Fig.32). In the model, LTG-01 will function as injection well and a second well (LTG-02) has been suggested as production well. The sequence boundary between cycle 2a and 2b is encountered at a depth of ± 4800 m, where temperatures of 190-200°C are expected, which would be sufficient for the generation of electricity (Fig.2). Both the fault plane and the sequence boundary have been proven to host increased porosity and may thus be pathways for fluid flow. To get a more detailed picture of the structure of the platform, the faults and the sequence boundaries, 3D seismic data should be shot in the area. This could lead to the creation of a more detailed model which could infer fluid flow through the fault zone and/or sequence boundaries. 3D seismic modeling could also help retrieve more information about possible induced seismicity that can be a result of fluid injection. If the sequence boundary could indeed be a pathway for geothermal fluids and the structure is mapped in detail, a geothermal flow field could be created which avoids the faulted zone, decreasing risk of induced seismicity. Also, more studies should be done to compute and monitor possible dissolution and precipitation of the carbonates (Blasco et al. 2017).

6.5 Uncertainties

The amount and quality of data available for investigating deep reservoirs, such as the Dinantian platforms in the Netherlands, are critical to the success of future related geothermal projects. This is based on the representivity of the available data with respect to the subsurface and their uncertain character. For instance; only 5.5m of slabbed core material from 800m thick reservoir could be

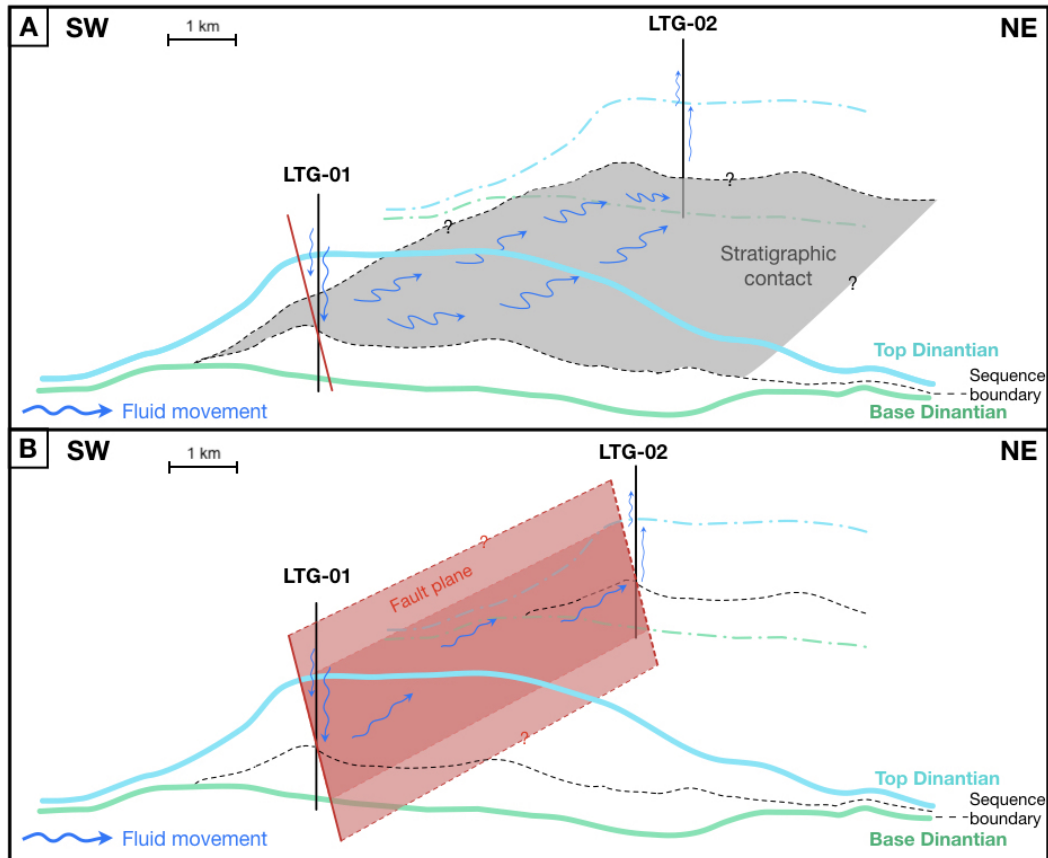


Figure 32: Proposed models for a geothermal system in the Luttelgeest carbonate platform: (A) Through stratigraphic contact (cycle 2a-2b); (B) Along a fault plane/zone. Blue arrows indicate the flow of geothermal fluids, where LTG-01 is the injector and proposed second well LTG-02 is the producer. 3D view of the area is uncertain, and is therefore indicated with dashed lines and question marks.

investigated in this study, which alone would not be meaningful. Yet by integrating core data, well logs, seismic data and analogue studies, reasonable geological models and trends might be proposed.

In addition, several uncertain parameters and issues need to be examined. For example the base of the Dinantian, which is not clearly defined in seismic data and in many studies still open to interpretation as descriptions are often conflicting with actual core data (Geluk et al. 2007). This is important for understanding the relation of faults running through the Dinantian rocks and the underlying sediments and possible fluid flows that occurred or can occur. Therefore, a revision of the Dinantian of the Dutch subsurface is required. Multiple studies have tried this (Fig.31; Geluk et al. 2007; Hoornveld 2013) but with no clear outcome.

Another parameter is the analysis of seismic facies. The major part of the well represents a high energy platform interior facies, which is in line with the seismic facies analysis in this study. Uncertainties exist about the chaotic facies in the platform, however. These have been interpreted as less well established platform interior sediments, but that could not be confirmed by well data due to lack of wells. Roksandić (1978) and Macurda et al. (1997) showed that chaotic seismic facies are typical for reef buildups, but correlation to nearby platforms showed that the existence of reef buildups on the Luttelgeest platform was unlikely (Mozafari et al. 2019). The chaotic facies could also be indicators of karst (Embry et al. 2020; Qi et al. 2020). This is however also unlikely since karst horizons only were observed in Dinantian platforms just north of the London Brabant Massif (e.g. well S02-02, where the karst body cuts down to the 2d sequence cycle). According to Van Hulten & Poty (2012), karst did not affect carbonate platforms in the north. These features are important for deeply buried carbonate platforms to be able to function as a reservoir rock.

7 Conclusions

Based on a thorough analysis of previous works, quantitative petrography on core data, log- and well-data and the interpretation of 2D seismic reflection data from the Luttelgeest platform, we advanced our understanding of the controls that affect the geothermal potential of the Dinantian reservoir rocks. The major results of the presented conceptual model are as follows:

- Quantitative petrography and FMI analysis showed that any porosity encountered in the rock is located in fractures or intracrystalline pore systems in veins. Fluid flow through the rock matrix is not feasible as porosity and permeability are close to zero here.
- Intracrystalline porosity in the vein-filling dolomite cement (SD2) was partially cemented by a later stage of calcite (C4). Quantitative petrography showed that the initial intracrystalline porosity used to be 9 to 17%, which is substantially higher than the current porosity (3 to 7%). If areas that have not been affected by the cementation of C4 can be found, they can function as flow pathways and can be used for application of geothermal energy.
- Quantitative petrography showed that the base 120 m of the well has increased dolomite content (up to 40%). Further research should find out whether these dolomites are genetically linked to the SD2 observed in the veins, which hosts the intracrystalline porosity. If a hydrothermal model could be improved to map the dolomitic bodies beyond well LTG-01, an assessment on the location of a second well can be given.
- Seismic interpretation showed that the margins of the platform host several fracture systems. The faulted margins of the platform are an interesting target for the application of geothermal energy as the fractures could be pathways for fluid flow. More research on the structural and diagenetic controls of the margins should be done to contradict or confirm this.
- Seismic interpretation with well data integration showed that a large fault is crossing the well at ± 4800 m depth, at the sequence boundary between cycles 2a and 2b. A fractured, porous interval is located here which could be targeted for geothermal purposes. Temperatures of 190-200°C are expected here, which would be sufficient for electricity generation. In addition, appliance of geothermal development in stratigraphic boundary layers is less risky compared to the use of fault planes. Further 3D research should be done to be able to map the structure in more detail and to infer whether fluid flow would occur over the fault plane and/or through the stratigraphic boundary.
- Uncertainties were mostly reduced due to integration of multiple data sources to propose reasonable geological models. However, certain issues, such as the base of the Dinantian, should still be examined.
- Listed conclusions from this study apply not only to the Luttelgeest carbonate platform but the outcomes can also serve follow-up studies or study cases on similar objects to the Luttelgeest platform.

Acknowledgements

My sincere thanks go out to my supervisors, Prof. dr. Fadi Henri Nader and Prof. dr. Rudy Swennen, for guiding me through this project. I would also like to greatly thank dr. Eva de Boever for being involved as a committee member of the project just as much as my supervisors. To all of you: thank you for your patience, support and positive comments during this research project. I benefited greatly from your massive wealth of knowledge and constructive feedback. I am very grateful that you took me on as a student and continued to have faith in me over the time. We were lucky to finally physically meet each other at the inauguration of Fadi, which was a great evening. I really enjoyed working with you and hope to do so again in the future!

Special thanks go out to Kees Geel (EBN) for his support and sharing his skills of the Petrel software. It is impressive how much you know about the Dutch subsurface! Without you, I could not have created this project in the way I did. I also would like to thank André Slupik for the preparation of material in the TNO core house and the interesting coffee talks there.

References

- Besly, B. M. (1998). Carboniferous. *Petroleum geology of the North Sea: basic concepts and recent advances*, 104-136.
- Blasco, M., Auqué, L. F., Gimeno, M. J., Acero, P., & Asta, M. P. (2017). Geochemistry, geothermometry and influence of the concentration of mobile elements in the chemical characteristics of carbonate-evaporitic thermal systems. The case of the Tiermas geothermal system (Spain). *Chemical Geology*, 466, 696-709.
- Bless, M. J. M., Bouckaert, J., Bouzet, P., Conil, R., Cornet, P., Fairon-Demaret, M., & Pirllet, H. (1976). Dinantian rocks in the subsurface North of the Brabant and Ardenno-Rhenish Massifs in Belgium, The Netherlands and the Federal Republic of Germany. *Mededelingen-Rijks Geologische Dienst*, 27(3), 81-193.
- Bless, M. J. M., Bouckaert, J., & Paproth, E. (1983). Recent exploration in pre-Permian rocks around the Brabant Massif in Belgium, the Netherlands and the Federal Republic of Germany. In *Petroleum Geology of the Southeastern North Sea and the Adjacent Onshore Areas* (pp. 51-62). Springer, Dordrecht.
- Bonté, D., Van Wees, J. D., & Verweij, J. M. (2012). Subsurface temperature of the onshore Netherlands: new temperature dataset and modelling. *Netherlands Journal of Geosciences*, 91(4), 491-515.
- Boxem, T., Veldkamp, J. G., & Van Wees, J. D. A. M. (2016). Ultra-diepe geothermie: Overzicht, inzicht & to-do ondergrond. *TNO report*, 10803.
- Breislín, C., Crowley, S., Banks, V. J., Marshall, J. D., Millar, I. L., Riding, J. B., & Hollis, C. (2020). Controls on dolomitization in extensional basins: An example from the Derbyshire Platform, UK. *Journal of Sedimentary Research*, 90(9), 1156-1174.
- Broothaers, M., Bos, S., Lagrou, D., Harcouët-Menou, V., & Laenen, B. (2019). Lower Carboniferous limestone reservoir in northern Belgium: structural insights from the Balmatt project in Mol. In *European Geothermal Congress Proceedings, The Hague*.
- Cameron, T. D. J. (1992). *The geology of the southern North Sea* (No. 7). Balogh Scientific Books.
- Cameron, N., & Ziegler, T. (1997). Probing the lower limits of a fairway: further pre-Permian potential in the southern North Sea. *Geological Society, London, Special Publications*, 123(1), 123-141.
- Carpentier, S., & Steeghs, P. (2016). New and advanced processing of existing reflection seismic data: surface data. In: IMAGE-D7.1: Active seismic at basement and sedimentary. Report for IMAGE FP7 EU programme, grant nr. 608553.
- Cocks, L. R. M., & Torsvik, T. H. (2005). Baltica from the late Precambrian to mid-Palaeozoic times: the gain and loss of a terrane's identity. *Earth-Science Reviews*, 72(1-2), 39-66.
- Collins, J., Narr, W., Harris, P. M., Playton, T., Jenkins, S., Tankersley, T. E. R. E. L. L., & Playton, T. E. (2013). Lithofacies, depositional environments, burial diagenesis, and dynamic field behavior in a Carboniferous slope reservoir, Tengiz Field (Republic of Kazakhstan), and

- comparison with outcrop analogs. *Deposits, Architecture, and Controls of Carbonate Margin, Slope, and Basinal Settings: SEPM, Special Publication, 105*, 50-83.
- Corfield, S. M., Gawthorpe, R. L., Gage, M., Fraser, A. J., & Besly, B. M. (1996). Inversion tectonics of the Variscan foreland of the British Isles. *Journal of the Geological Society, 153*(1), 17-32.
- Cornford, C. (1998). Source rocks and hydrocarbons of the North Sea. *Petroleum geology of the North Sea: Basic concepts and recent advances*, 376-462.
- Coward, M. P. (1993). The effect of Late Caledonian and Variscan continental escape tectonics on basement structure, Paleozoic basin kinematics and subsequent Mesozoic basin development in NW Europe. In *Geological Society, London, Petroleum Geology Conference Series* (Vol. 4, No. 1, pp. 1095-1108). Geological Society of London.
- De Jager, J., Geluk, M. C., Wong, T. E., & Batjes, D. A. J. (2007). Geology of the Netherlands. *Petroleum Geology. Royal Netherlands Academy of Arts and Sciences, Amsterdam, The Netherlands, 241*, 264
- Drozdowski, G. (2005). Zur sedimentären Entwicklung des Subvariscikums im Namurium und Westfalium Nordwestdeutschlands. *Courier-Forschungsinstitut Senckenberg, 254*, 271.
- Embry, J. C., Hunt, D., Colpaert, A., Dræge, A., & Zahm, L. (2020). Seismic facies, stratigraphy, geomorphology, and seismic modelling of a Lower Cretaceous carbonate platform. *Geological Society, London, Special Publications, 509*.
- Franke, W. (2000). The mid-European segment of the Variscides: tectonostratigraphic units, terrane boundaries and plate tectonic evolution. *Geological Society, London, Special Publications, 179*(1), 35-61.
- Fraser, A. J., & Gawthorpe, R. L. (1990). Tectono-stratigraphic development and hydrocarbon habitat of the Carboniferous in northern England. *Geological Society, London, Special Publications, 55*(1), 49-86.
- Haq, B. U., & Schutter, S. R. (2008). A chronology of Paleozoic sea-level changes. *Science, 322*(5898), 64-68.
- Harris, P. M. (2008). Geologic Framework for the Tengiz and Korolev Fields, Kazakhstan–Carboniferous Isolated Carbonate Platforms. *American Association of Petroleum Geologists*.
- Hollis, C., & Walkden, G. (1996). The use of burial diagenetic calcite cements to determine the controls upon hydrocarbon emplacement and mineralization on a carbonate platform, Derbyshire, England. *Geological Society, London, Special Publications, 107*(1), 35-49.
- Hollis, C. (1998). Reconstructing fluid history: an integrated approach to timing fluid expulsion and migration on the Carboniferous Derbyshire Platform, England. *Geological Society, London, Special Publications, 144*(1), 153-159.
- Hollis, C., & Walkden, G. (2012). Burial diagenetic evolution of the Lower Carboniferous (Dinantian) of the southern margin of the Askrigg Platform and a comparison with the Derbyshire Platform. *Petroleum Geoscience, 18*(1), 83-95.
- Hoornveld, N. (2013). Dinantian carbonate development and related prospectivity of the onshore Northern Netherlands. *Vrije Universiteit Amsterdam (Amsterdam)*.
- Kombrink, H. (2008). *The Carboniferous of the Netherlands and surrounding areas; a basin analysis. Geologica Ultraiectina (294)*. Departement Aardwetenschappen.
- Macurda, D. B., Palaz, I., & Marfurt, K. J. (1997). Carbonate seismic facies analysis. *Carbonate seismology: Geophysical development series: Tulsa, Oklahoma, Society of Exploration Geophysicists, 6*, 95-119.
- Mijnlieff, H. F. (2020). Introduction to the geothermal play and reservoir geology of the Netherlands. *Netherlands Journal of Geosciences, 99*.
- Mozafari, M., Gutteridge, P., Riva, A., Geel, K., Garland, J. & Dewit, J., (2019). Facies analysis and diagenetic evolution of the Dinantian carbonates in the Dutch subsurface. SCAN report. Energie Beheer Nederland B.V. (EBN) (Utrecht).
- Muchez, P., Viaene, W., & Marshall, J. D. (1991a). Origin of shallow burial cements in the Late Viséan of the Campine Basin, Belgium. *Sedimentary Geology, 73*(3-4), 257-271.
- Muchez, P., Viaene, W. A., Keppens, E., Marshall, J. D., & Vandenberghe, N. (1991b). Vein cements and the geochemical evolution of subsurface fluids in the Viséan of the Campine Basin (Poederlee borehole, Belgium). *Journal of the Geological Society, 148*(6), 1005-1117.

- Narkiewicz, M. (2007). Development and inversion of Devonian and Carboniferous basins in the eastern part of the Variscan foreland (Poland). *Geological Quarterly*, 51, 231-256.
- Ortega, O. J., Gale, J. F., & Marrett, R. (2010). Quantifying diagenetic and stratigraphic controls on fracture intensity in platform carbonates: An example from the Sierra Madre Oriental, northeast Mexico. *Journal of Structural Geology*, 32(12), 1943-1959.
- Papadimitriou, N., Gorini, C., Nader, F. H., Deschamps, R., Symeou, V., & Lecomte, J. C. (2018). Tectono-stratigraphic evolution of the western margin of the Levant Basin (offshore Cyprus). *Marine and Petroleum Geology*, 91, 683-705.
- Pharaoh, T. C. (1999). Palaeozoic terranes and their lithospheric boundaries within the Trans-European Suture Zone (TESZ): a review. *Tectonophysics*, 314(1-3), 17-41.
- Poty, E., Hance, L., Lees, A., & Hennebert, M. (2002). Dinantian lithostratigraphic units (Belgium). *Geologica Belgica*, 4(1/2), 69-94.
- Qi, Jie, Bo Zhang, Bin Lyu, and Kurt Marfurt. "Seismic attribute selection for machine-learning-based facies analysis." *Geophysics* 85, no. 2 (2020): O17-O35.
- Reijmer, J. J., Johan, H., Jaarsma, B., & Boots, R. (2017). Seismic stratigraphy of Dinantian carbonates in the southern Netherlands and northern Belgium. *Netherlands Journal of Geosciences*, 96(4), 353-379.
- Reith, D. (2018). Dynamic simulation of a geothermal reservoir: case study of the Dinantian carbonates in the Californië geothermal wells, Limburg, NL.
- Roksandić, M. M. (1978). Seismic facies analysis concepts. *Geophysical prospecting*, 26(2), 383-398.
- Ronchi, P., Ortenzi, A., Borromeo, O., Claps, M., & Zempolich, W. G. (2010). Depositional setting and diagenetic processes and their impact on the reservoir quality in the late Viséan–Bashkirian Kashagan carbonate platform (Pre-Caspian Basin, Kazakhstan). *AAPG bulletin*, 94(9), 1313-1348.
- Sarg, J. F. (1988). Carbonate sequence stratigraphy.
- Schroot, B. M., Van Bergen, F., Abbink, O. A., David, P., Van Eijs, R., & Veld, H. (2006). Hydrocarbon potential of the Pre-Westphalian in the Netherlands on-and offshore—report of the Petro-Play project. *TNO Built Environment and Geosciences Report NITG-05-155-C*.
- Schulmann, K., Catalán, J. R. M., Lardeaux, J. M., Janoušek, V., & Oggiano, G. (2014). The Variscan orogeny: extent, timescale and the formation of the European crust. *Geological Society, London, Special Publications*, 405(1), 1-6.
- Sissingh, W. (2004). Palaeozoic and Mesozoic igneous activity in the Netherlands: a tectono-magmatic review. *Netherlands Journal of Geosciences*, 83(2), 113-134.
- Ter Borgh, M. M., Jaarsma, B., & Rosendaal, E. A. (2019). Structural development of the northern Dutch offshore: Paleozoic to present. *Geological Society, London, Special Publications*, 471(1), 115-131.
- Vachard (2004). Cuttings descriptions LTG-01. 5p.
- Van Adrichem Boogaert, H. A., & Kouwe, W. F. (1997). Stratigraphic Nomenclature of the Netherlands, Revision and Update by RGD and NOGEPa, Meded. *Rijks Geol. Dienst*, 50.
- Van der Hoorn, K., Heijnen, L. J., Gankema, M. E., & Nitters, G. (2012). Hydraulic fracturing in limestone: A case study of two EGS Projects in the Netherlands. In *Proceedings, Thirty-Seventh Workshop on Geothermal Reservoir Engineering*.
- Van Hulst, F. F. N., & Poty, E. (2008). Geological factors controlling Early Carboniferous carbonate platform development in the Netherlands. *Geological Journal*, 43(2-3), 175-196.
- Van Hulst, F. F. N., & Poty, E. (2009). Dinantian reefs underneath the Netherlands. In *71st EAGE Conference and Exhibition incorporating SPE EUROPEC 2009* (pp. cp-127). European Association of Geoscientists & Engineers.
- Van Hulst, F. F. N. (2012). Devonian-carboniferous carbonate platform systems of the Netherlands. *Geologica Belgica*.
- Van Leverink, D., & Geel, K. (2019). Fracture characterization of the Dinantian carbonates in the Dutch subsurface. SCAN report. Energie Beheer Nederland B.V. (EBN) (Utrecht).
- Van Oversteeg, K., Lipsey, L., Pluymaekers, M., Van Wees, J. D., Fokker, P. A., & Spiers, C. (2014, February). Fracture Permeability Assessment in Deeply Buried Carbonates and Implications for Enhanced Geothermal Systems: Inferences from a Detailed Well Study at Luttelgeest-

- 01, The Netherlands. In *Proceedings Thirty-Eighth Workshop on Geothermal Reservoir Engineering, Stanford University, Stanford, California*.
- Walkden, G. M., & Williams, D. O. (1991). The diagenesis of the late Dinantian Derbyshire-East Midland carbonate shelf, central England. *Sedimentology*, 38(4), 643-670.
- Weber, L. J., Francis, B. P., Harris, P. M., & Clark, M. (2003). Stratigraphy, lithofacies, and reservoir distribution, Tengiz Field, Kazakhstan.
- Ziegler, P. A. (1990). Geological atlas of western and central Europe. Geological Society of London.

Appendices

Appendix A: Lithostratigraphic nomenclature of the Dutch Dinantian

All information in this subsection comes from the NLOG-website (<https://www.nlog.nl/>).

Introduction

The term Dinantian refers to a regional series for Lower Carboniferous sediment succession in the region of Belgium, the Netherlands and neighbouring countries (Groessens 1989; 2006). The Dinantian successions are defined as Farne and Carboniferous limestone groups in offshore and onshore Netherlands respectively (Kombrink 2008 and references therein). The top of the Dinantian is quite clear in onshore areas in the Netherlands and roughly corresponds to the top of the Zeeland formation (Visean; Mozafari et al. 2019). The base, however, has not yet been clearly defined.

Carboniferous limestone group

In the study area, this group consists of the Zeeland formation: Mainly light-grey to brownish and black limestones, and medium- grey to dark-brown dolomites. Intercalations of thin to medium-thick fissile claystone and chert beds are common. The top of the formation has been placed where the calcareous deposits change into the finer clastics of the Silesian. This boundary is in many places a sharp contact. However, in areas where the Zeeland formation was truncated by later erosion, the upper part of the formation may be strongly leached and subsequently karstified and younger sediments may overlie unconformably. The base of the Zeeland formation is formed by the contact with the clastic sediments of the earliest Carboniferous formation or the Late Devonian Bollen claystone. The Zeeland formation is subdivided in three members: The Goeree, the Schouwen and the Beveland member, which are described below:

Goeree member

The Goeree member comprises a sequence of grey to dark-grey and black limestones, which are thin- to thick-bedded and often partly silicified. The limestone beds often grade into calcareous and/or silicified black shales or black cherts toward the top. Very thin beds of tuffaceous rock occur, predominantly in the upper part of the member.

Schouwen member

The Schouwen member comprises a thick sequence of light to dark-grey, dark- to yellowish-brown and brownish-black, and light yellowish- brown to dusty yellow-brown limestones. The dense limestones are micritic, biosparitic to biomicritic, locally oolitic and abundantly fossiliferous. The limestones are dolomitized, especially near fault zones, or silicified in the leached zone in areas where later erosion truncated the formation.

Beveland member

The Beveland member comprises a sequence of brown grey to brown-black, coarse-crystalline dolomites, often containing black organic intergranular residues. The dolomites are generally of secondary origin. In places minor grey to dark-grey limestone intercalations occur, as well as minor quantities of dark-brown to blackish siltstone and shaly claystone. In addition, dark beds of silicified dolomite are occasionally present.

Farne group

The Farne group can be seen as the offshore version of the Carboniferous limestone group. It consists of claystones and sandstones with minor coal seams, and a variable amount of intercalated limestone and dolomite beds. The top of the group has been placed at the top of the highest limestone. In areas subjected to later erosion, the group is overlain unconformably by younger formations (Rotliegend to Chalk). The group overlies the Old Red group conformably. Its base is marked by the lowermost

carbonate bed. The Farne group consists of the Yoredale, Elleboog and the Cementstone formation, which are described below:

Yoredale formation

The Yoredale formation comprises a cyclic alternation of limestones, claystones, sandstones and rarely some coal seams. The upper boundary is defined by the top of the uppermost limestone bed. The formation is overlain conformably by the Silesian sediments, which locally contain some minor carbonate intercalations in its basal part. The lower boundary has been placed at the base of the first distinct limestone bed overlying the clastics of the Elleboog formation.

Elleboog formation

The Elleboog formation comprises a sequence of alternating claystones, sandstones and minor amounts of coal, with a few calcareous or dolomitic intercalations. The amount of sandstone tends to increase westward. The upper boundary is at the base of the lowermost limestone bed of the overlying Yoredale formation. The lower boundary has been placed at the top of the uppermost carbonate bed of the underlying Cementstone formation.

Cementstone formation

The Cementstone formation comprises a cyclic alternation of carbonates, claystones, sandstones and minor coal seams. The carbonates occur as limestone, dolomitic limestone and dolomite beds.

Appendix B: Quantitative petrography results

Quantitative petrography on rock matrix

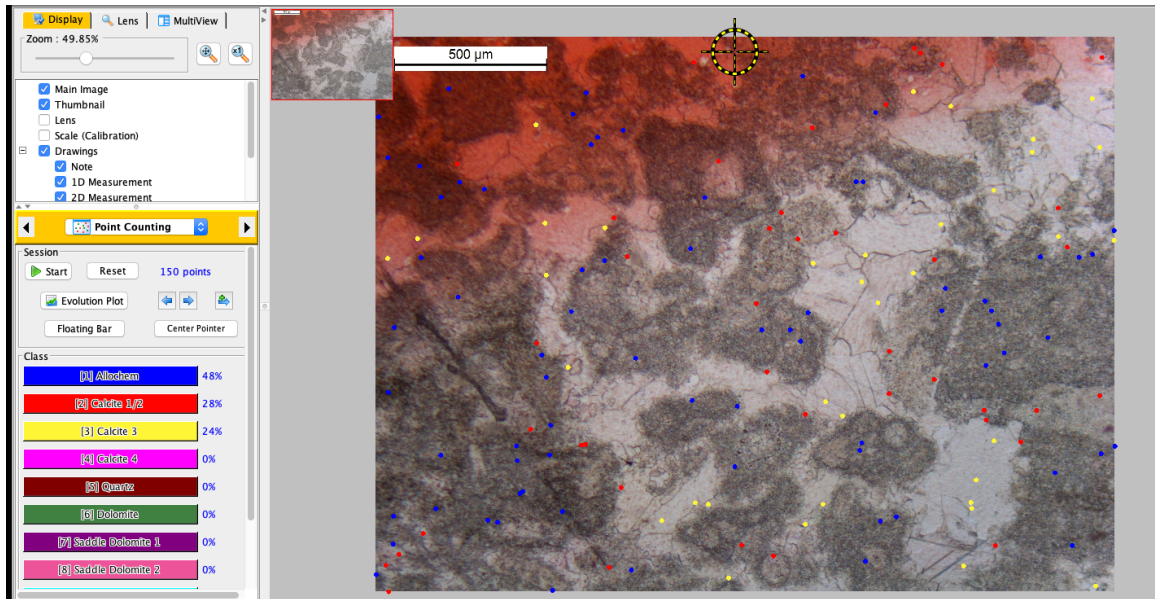


Figure 33: Matrix point counting on sample LTG-01_4470_30m-1. Results are shown in the bottom left corner.

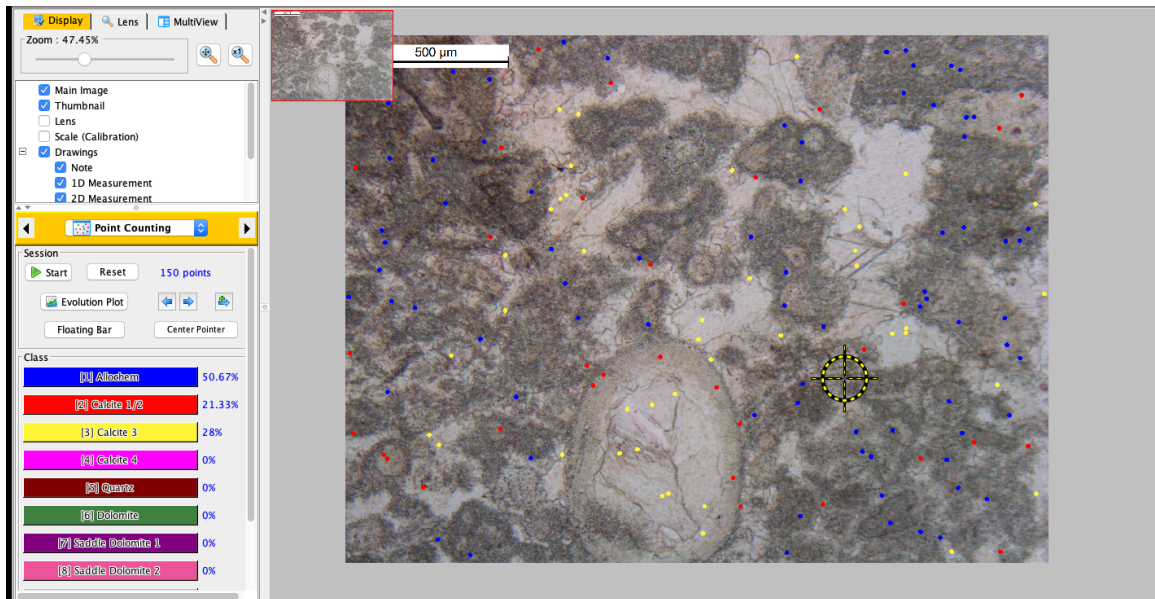


Figure 34: Matrix point counting on sample LTG-01_4470_30m-2. Results are shown in the bottom left corner.

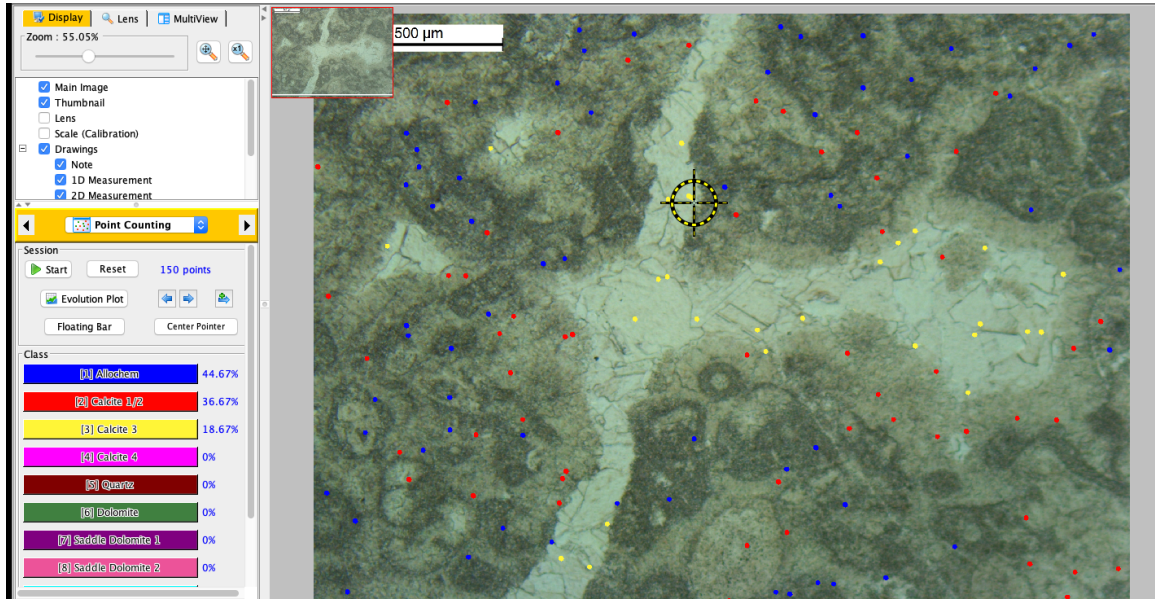


Figure 35: Matrix point counting on sample LTG-01_4471_92m-1. Results are shown in the bottom left corner.

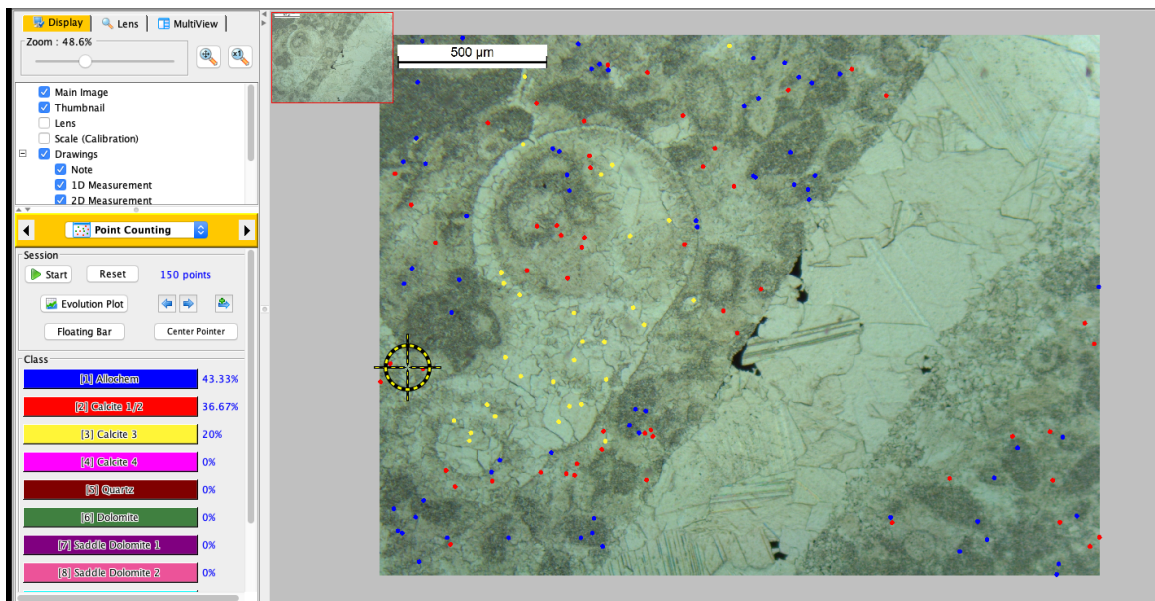


Figure 36: Matrix point counting on sample LTG-01_4471_92m-2. Results are shown in the bottom left corner.

Quantitative petrography on vein infill

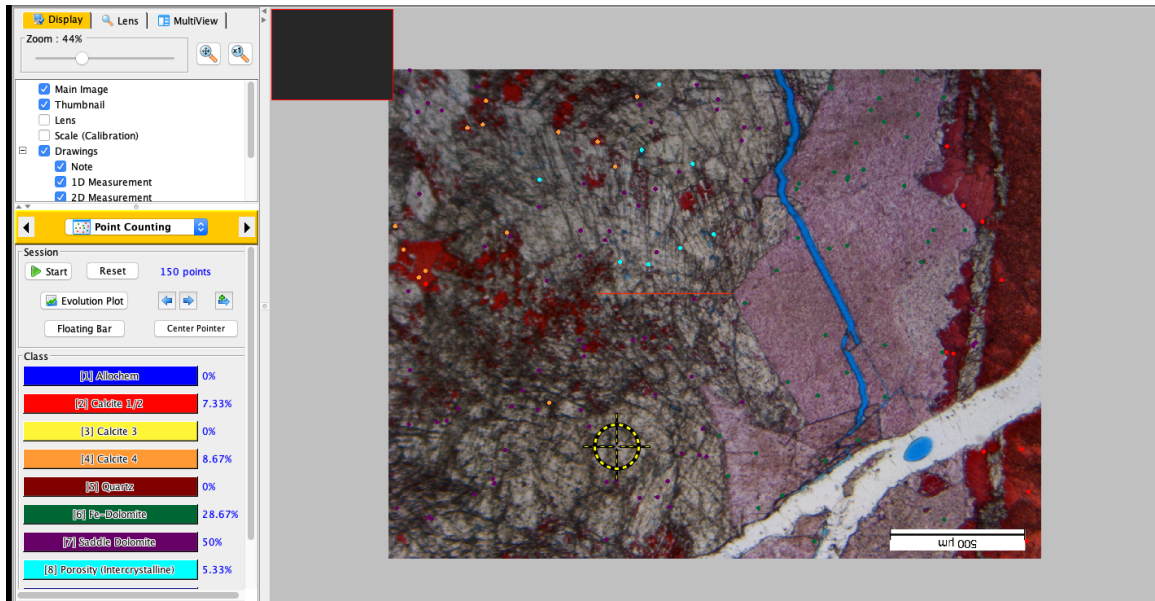


Figure 37: Vein infill point counting on sample LTG-01_4470_30m-3. Results are shown in the bottom left corner.

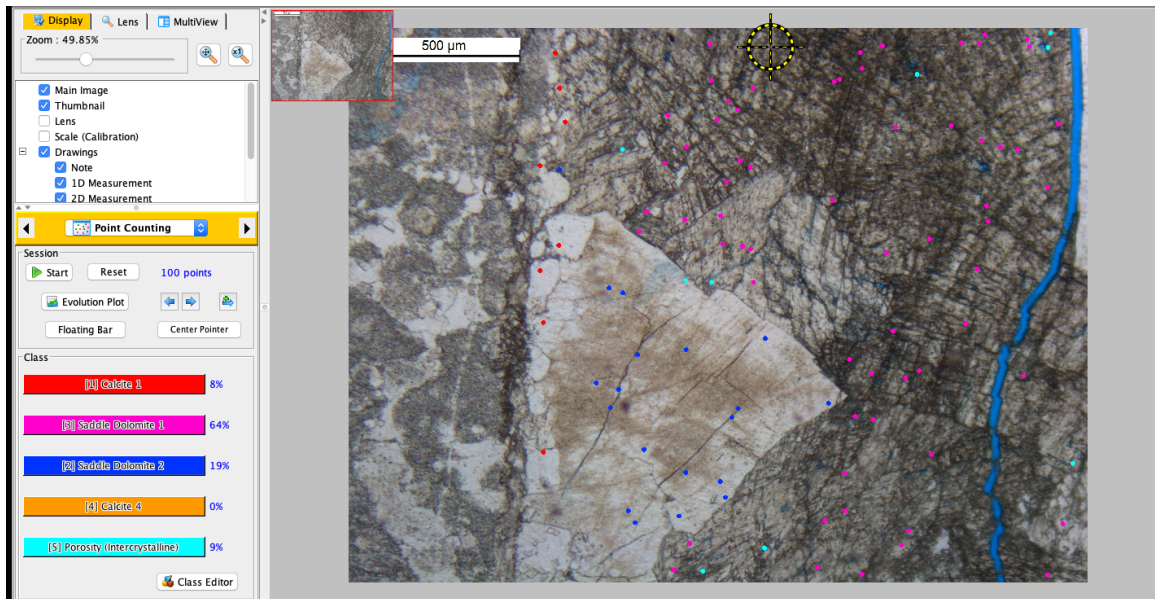


Figure 38: Vein infill point counting on sample LTG-01_4470_30m-4. Results are shown in the bottom left corner.

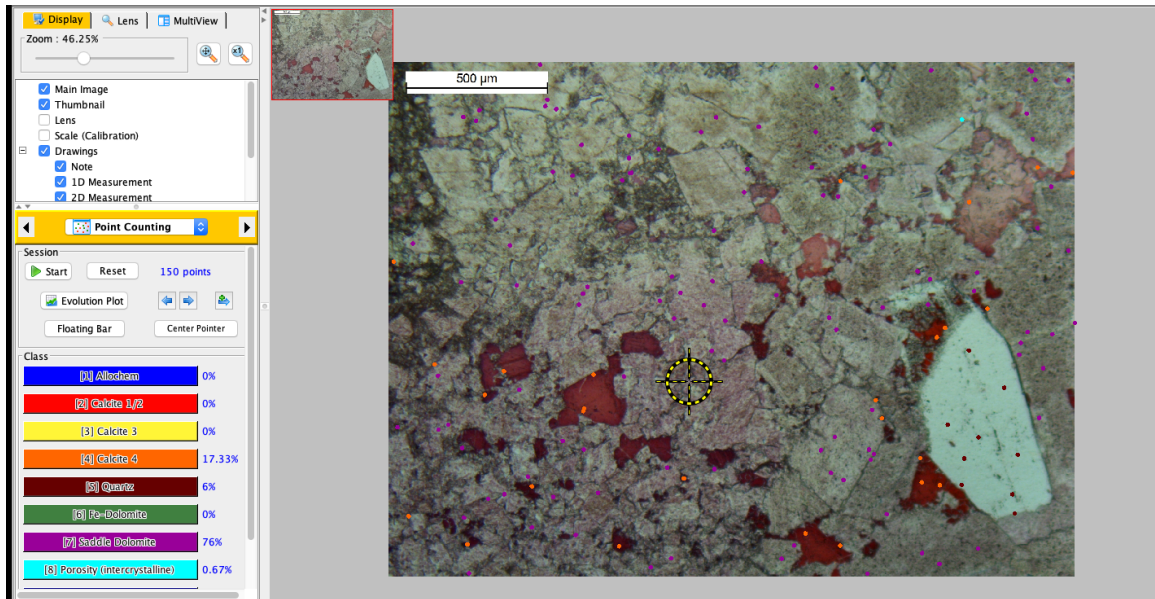


Figure 39: Vein infill point counting on sample LTG-01_4470_63m-1. Results are shown in the bottom left corner.

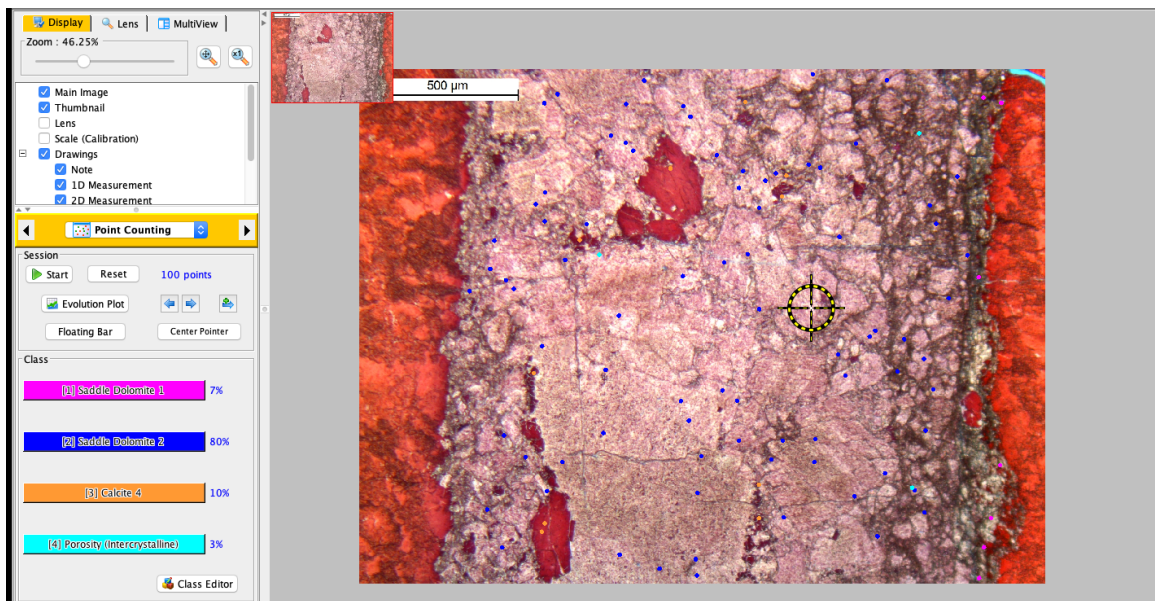


Figure 40: Vein infill point counting on sample LTG-01_4470_63m-2. Results are shown in the bottom left corner.

Quantitative petrography on cuttings

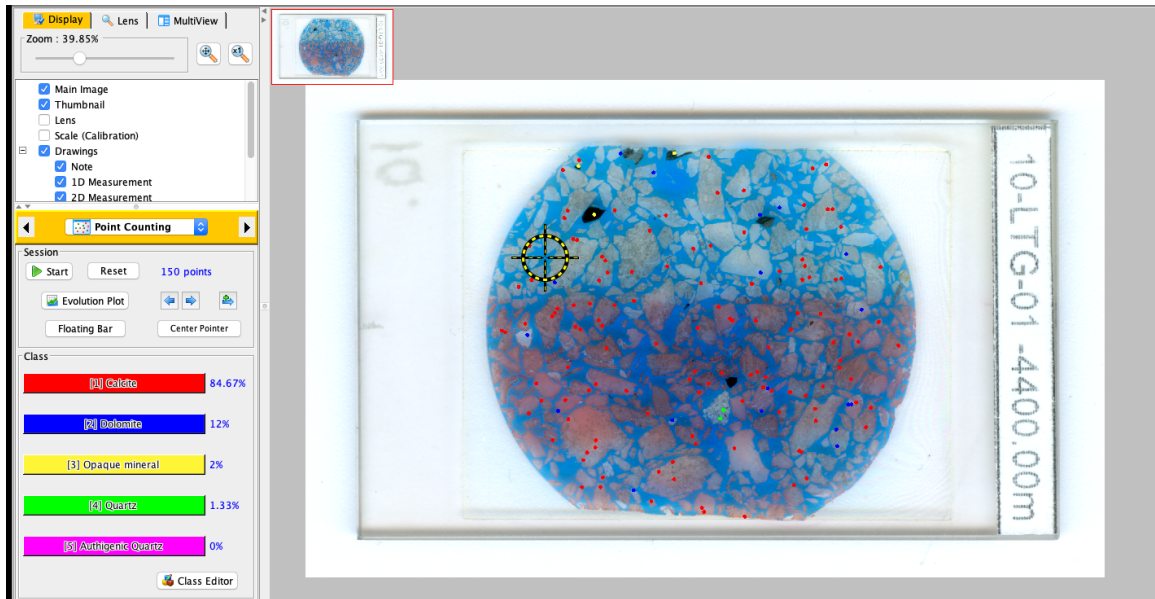


Figure 41: *Cuttings point counting on sample 10-LTG-01 (depth: 4400m). Results are shown in the bottom left corner.*

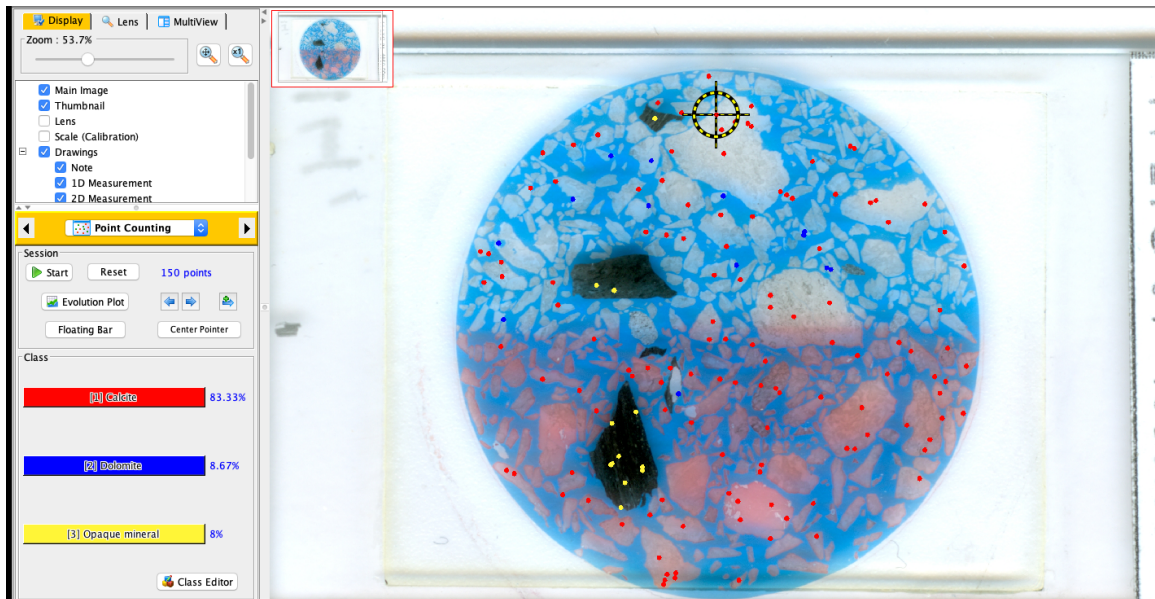


Figure 42: *Cuttings point counting on sample 14-LTG-01 (depth: 4600m). Results are shown in the bottom left corner.*

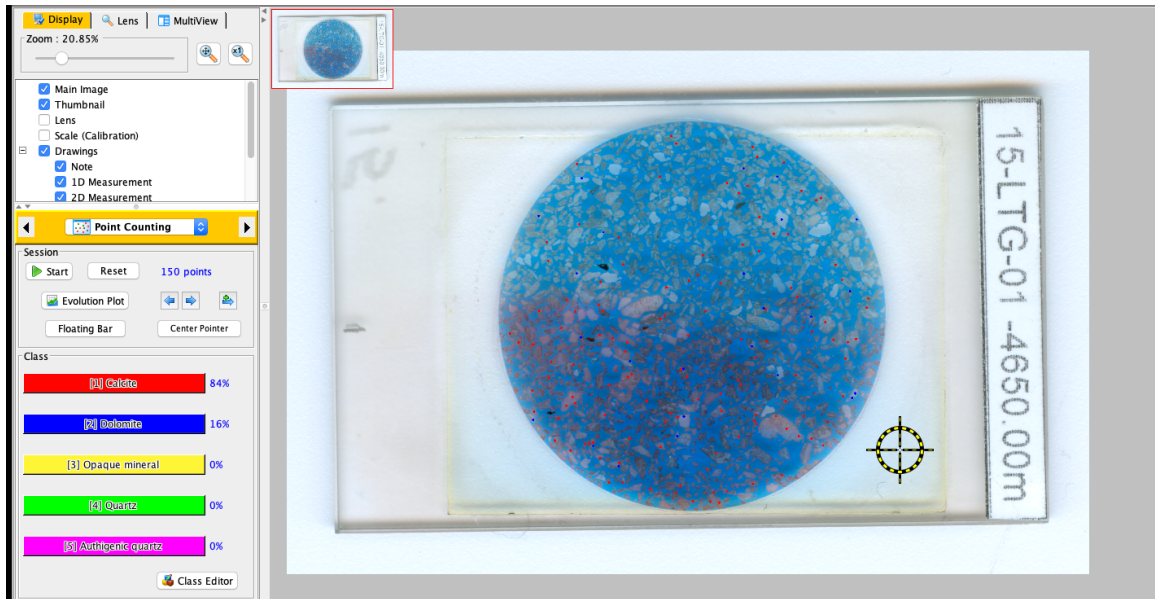


Figure 43: Cuttings point counting on sample 15-LTG-01 (depth: 4650m). Results are shown in the bottom left corner.

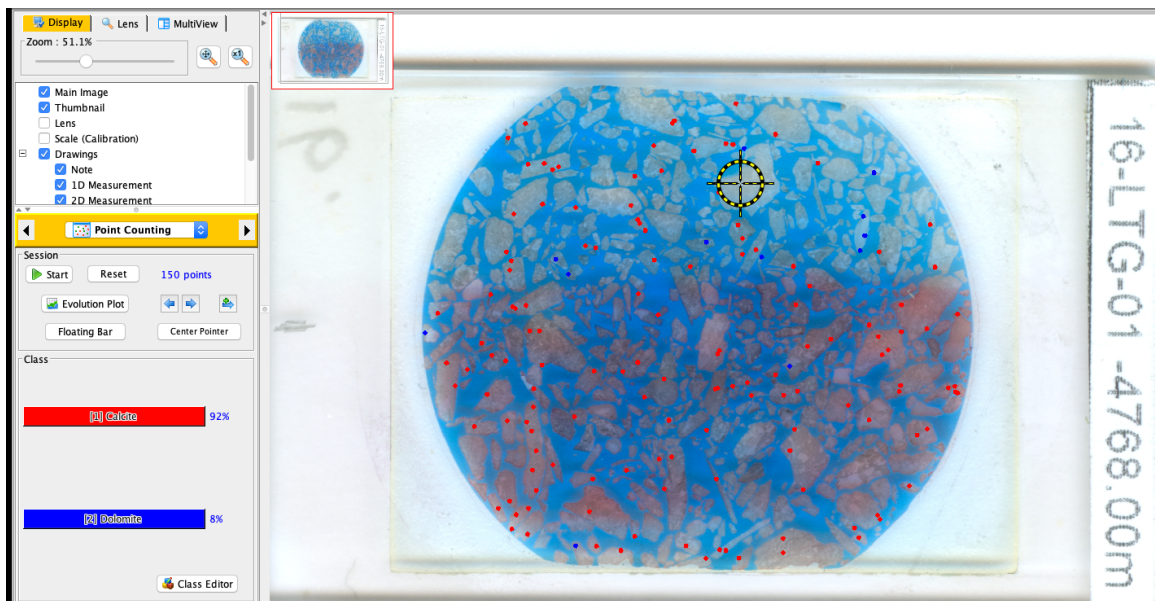


Figure 44: Cuttings point counting on sample 16-LTG-01 (depth: 4768m). Results are shown in the bottom left corner.



Figure 45: Cuttings point counting on sample 17-LTG-01 (depth: 4800m). Results are shown in the bottom left corner.

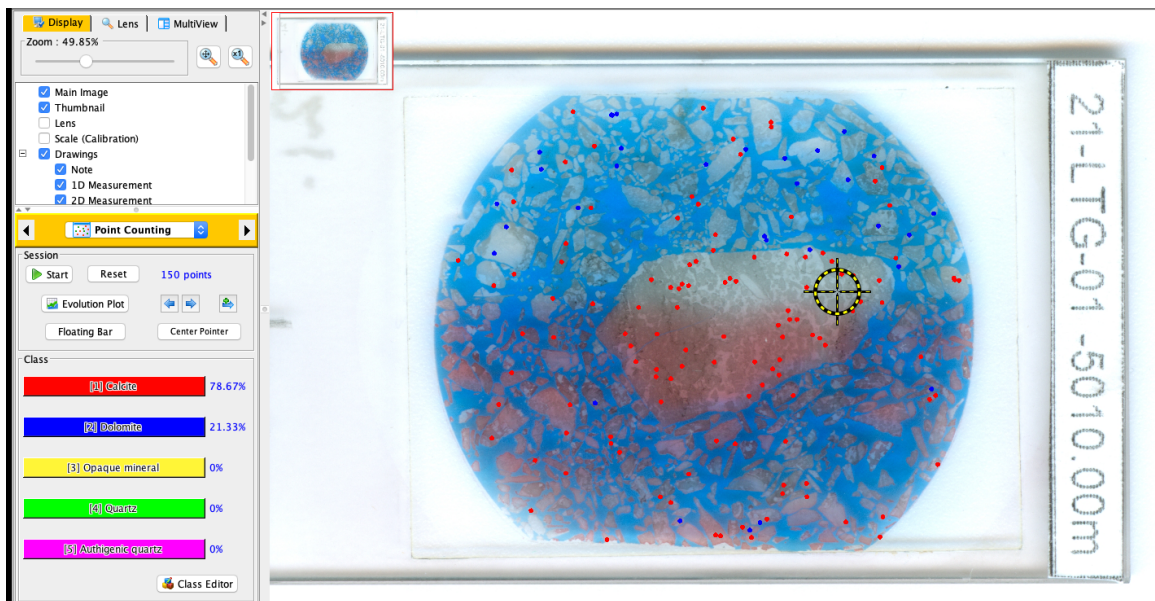


Figure 46: Cuttings point counting on sample 21-LTG-01 (depth: 5010m). Results are shown in the bottom left corner.

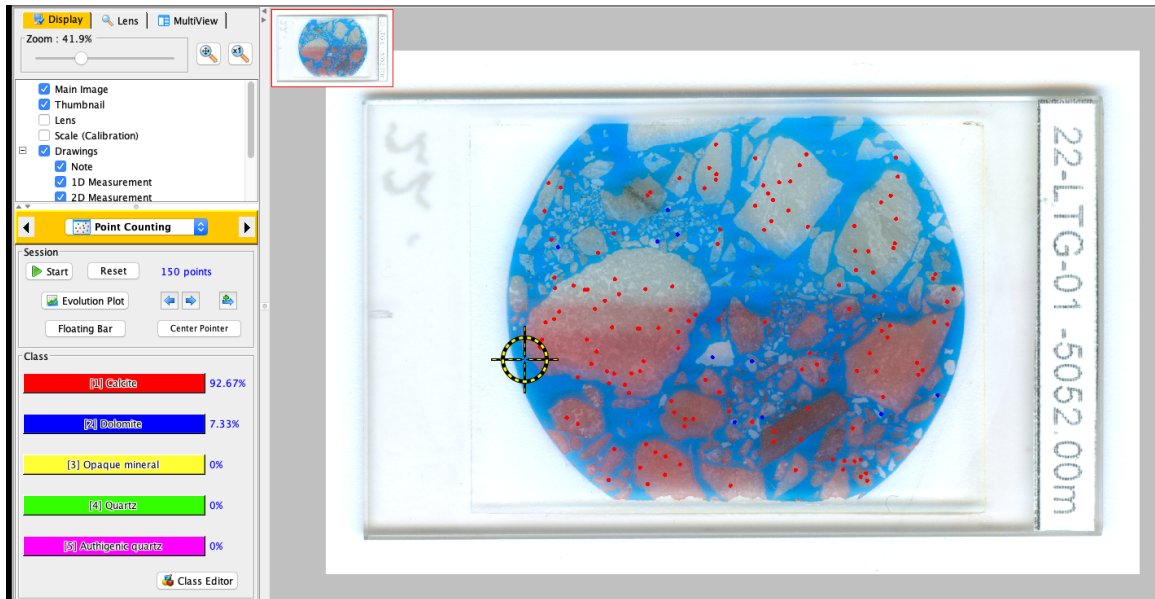


Figure 47: Cuttings point counting on sample 22-LTG-01 (depth: 5052m). Results are shown in the bottom left corner.

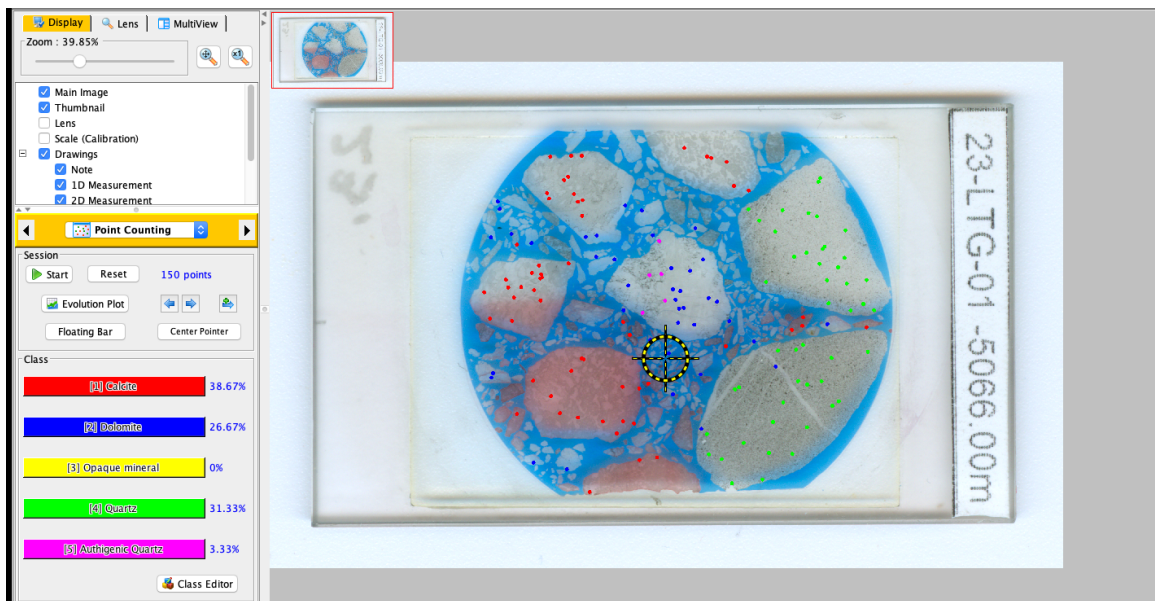


Figure 48: Cuttings point counting on sample 23-LTG-01 (depth: 5066m). Results are shown in the bottom left corner.

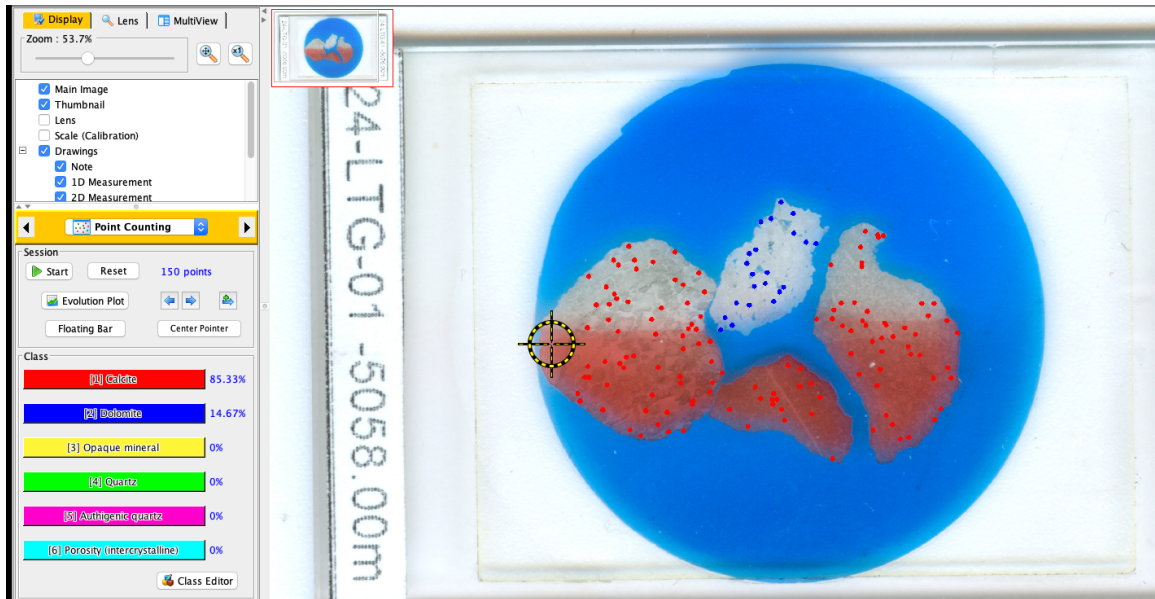


Figure 49: Cuttings point counting on sample 24-LTG-01 (depth: 5058m). Results are shown in the bottom left corner.

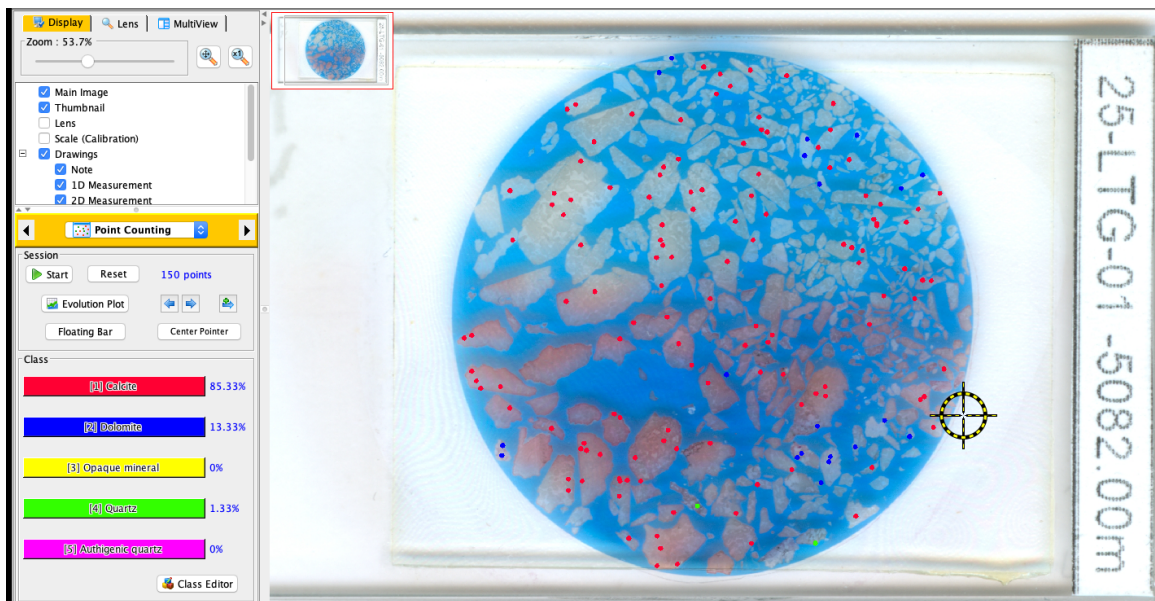


Figure 50: Cuttings point counting on sample 25-LTG-01 (depth: 5082m). Results are shown in the bottom left corner.